ADAMTS7 promotes smooth muscle foam cell expansion in atherosclerosis

Allen Chung[1], Hyun K. Chang[1], Huize Pan[1, 2], Alexander C. Bashore[1, 3], Karissa Shuck[1], Caio V. Matias[1], Juliana Gomez[1], Hanying Yan[4], Mingyao Li[4], Robert C. Bauer[1]*

[1]Cardiometabolic Genomics Program, Division of Cardiology, Department of Medicine, Columbia University, New York, NY, USA

[2]Division of Cardiovascular Medicine, Department of Medicine, Vanderbilt University Medical Center, Nashville, TN, USA

[3]Cardiovascular Research Institute, Icahn School of Medicine at Mount Sinai, New York, NY, USA

[4]Department of Biostatistics, Epidemiology and Informatics, University of Pennsylvania Perelman School of Medicine, Philadelphia, PA, USA

***Correspondence to**

Robert C. Bauer, Ph.D.

630 W. 168th Street, PS10-401,

New York, NY 10032, USA.

E-mail: rcb36@columbia.edu

The authors have declared that no conflict of interest exists.

ABSTRACT

Human genetic studies have repeatedly associated *ADAMTS7* with atherosclerotic cardiovascular disease. Subsequent investigations in mice demonstrated that ADAMTS7 is proatherogenic and induced in response to vascular injury and that the proatherogenicity of ADAMTS7, a secreted protein, is due to its catalytic activity. However, the cell-specific mechanisms governing ADAMTS7 proatherogenicity remain unclear. To determine which vascular cell types express *ADAMTS7*, we interrogated single-cell RNA sequencing of human carotid atherosclerosis and found *ADAMTS7* expression in smooth muscle cells (SMCs), endothelial cells (ECs), and fibroblasts. We subsequently created SMC- and EC-specific *Adamts7* conditional knockout and transgenic mice. Conditional knockout of *Adamts7* in either cell type is insufficient to reduce atherosclerosis, whereas transgenic induction in either cell type increases atherosclerosis. In SMC transgenic mice, this increase coincides with an expansion of lipid-laden SMC foam cells and decreased fibrous cap formation. RNA-sequencing in SMCs revealed an upregulation of lipid uptake genes typically assigned to macrophages. Subsequent experiments demonstrated that ADAMTS7 increases SMC oxLDL uptake through increased CD36 levels. Furthermore, *Cd36* expression is increased due to increased levels of PU.1, a transcription factor typically associated with myeloid fate determination. In summary, *Adamts7* expression in either SMCs or ECs promotes SMC foam cell formation and atherosclerosis. In SMCs, ADAMTS7 promotes oxLDL uptake via increased PU.1 and *Cd36* expression, thereby increasing SMC foam cell formation and atherosclerosis.

INTRODUCTION

Coronary artery disease (CAD) is the leading cause of death in the United States despite the widespread availability of multiple highly effective lipid-lowering therapies (1). Thus, there is a need for novel non-lipid lowering therapeutic approaches for the treatment of CAD. Human genome-wide association studies (GWAS) have proven an effective, unbiased approach to discovering novel genomic loci associated with CAD, potentially uncovering novel therapeutic targets. GWAS have repeatedly identified the 15q25 locus as a region of interest for CAD (2-5). This locus harbors the gene A disintegrin and metalloproteinase with thrombospondin motifs 7 (*ADAMTS7*), which encodes a secreted matrix metalloproteinase previously implicated in osteoarthritis (6). After its identification by GWAS, subsequent mouse studies demonstrated that ADAMTS7 is proatherogenic, as mice with whole-body *Adamts7* knockout had reduced atherosclerosis (7). Notably, this reduction in atherosclerosis occurred without any changes in plasma lipoprotein levels, suggesting that ADAMTS7 has a lipid-independent role in atherogenesis (8). Further mouse models of *Adamts7* have confirmed this proatherogenicity while demonstrating that ADAMTS7 catalytic activity is required for this effect (9, 10). Given these findings, ADAMTS7 is an attractive lipid-independent therapeutic target for treating CAD, but questions remain regarding the molecular mechanisms underlying the association between *ADAMTS7* and CAD.

There has recently been an increased appreciation for the role of smooth muscle cells (SMCs) in atherosclerosis (11). Historically, SMCs were considered to exclusively contribute to forming the fibrous cap during atherosclerosis. However, advances in single-cell technology employing lineage tracing approaches have revealed that SMCs can undergo phenotypic modulation and acquire macrophage-like characteristics (12, 13). Additionally, studies in the *Apoe*^{KO} model of atherosclerosis revealed that most lipid-laden foam cells are not macrophages but cells of SMC origin, indicating that SMC foam cells play a more significant role in atherogenesis than previously understood (14). Mechanistic studies of ADAMTS7 have previously centered on its role in modulating SMC function, as *Adamts7* knockout and overexpression can alter both neointima formation following vascular injury and SMC migration in ex vivo

assays (7, 15). As ADAMTS7 is a secreted protein, it could affect SMC function while being expressed by neighboring cells (16). *Adamts7* is not constitutively expressed in vascular cells, but rather, its expression is induced in response to vascular injury and cytokine signaling (7, 9). The low basal expression of *Adamts7* in vivo and its transient nature after induction have dampened efforts to identify *Adamts7*'s causal cell type (7). Overall, ADAMTS7 has consistently been linked to SMC function, yet the mechanistic basis by which this association promotes atherosclerosis remains unknown (8).

In this study, we identified *ADAMTS7* expression in multiple human vascular cell types, including SMCs and endothelial cells (ECs). Additionally, we generated several novel tissue-specific *Adamts7* mouse models, allowing for mechanistic studies of ADAMTS7 during sustained induction or knockout. We demonstrate that conditional knockout of *Adamts7* in either SMCs or ECs alone does not reduce atherosclerosis. In contrast, SMC or EC overexpression increases atherosclerosis and SMC foam cell formation. We found in primary SMCs that *Adamts7* induction increases the expression of the myeloid transcription factor PU.1, increasing *Cd36* expression and SMC oxidized low-density lipoprotein (oxLDL) uptake. In conclusion, we show that ADAMTS7 promotes SMC foam cell expansion and, ultimately, atherosclerosis.

RESULTS

ADAMTS7 is induced within multiple vascular cell types during lesion formation

Prior literature indicates that *Adamts7* expression is induced within the vasculature and promotes SMC migration while inhibiting reendothelialization (7, 17). ADAMTS7 is secreted, and as such, the cell type that responds to it does not necessarily have to produce it. Thus, to determine the cellular origins of ADAMTS7, we interrogated the largest human atherosclerotic carotid artery scRNAseq dataset generated to date (18) and found that multiple vascular cell types express *ADAMTS7* in mature plaques. The highest *ADAMTS7* expression was present in ECs, whereas SMCs, fibroblasts, and mast cells

displayed *ADAMTS7* expression at a lower level. (Figure 1A). Interestingly, the highest level of *ADAMTS7* expression occurred in ECs annotated as inflammatory (18), whereas fibrotic ECs did not display as high a level of expression.

We next sought to confirm this observation in mouse models of atherosclerosis. Previous work in *Apoe*^{KO} mice has shown that *Adamts7* expression is induced after four weeks of western-type diet (WTD) feeding but absent by terminal time points (7). To determine when *Adamts7* is expressed during atherosclerosis, we performed RNAscope within the brachial cephalic artery (BCA) of hyperlipidemic Low-Density Lipoprotein Receptor knockout (*Ldlr*^{KO}) mice at four, six, and nine weeks of WTD. *Adamts7* expression appears during early atheroma formation and is especially prominent at nine weeks when established lesions are present (Figure 1B). Across multiple experiments, *Adamts7* expression localized to the developing atherosclerotic neointima and multiple other locations in the BCA, consistent with expression in SMCs and other cells (Figure 1B-D). To confirm EC expression as seen in the human scRNAseq data, we performed RNAscope in the BCA of *Ldlr*^{KO} mice after seven and ten weeks of WTD (Figure 1C and Figure 1D). At the early lesion time point of seven weeks, we detected colocalization of the *Adamts7* transcript with *Pecam1*, an EC marker, and at the ten-week time point, both ECs and non-ECs showed expression of *Adamts7*. These data support the notion that multiple vascular cell types produce ADAMTS7 during atherosclerosis in mice and humans.

SMC or EC specific knockout of *Adamts7* does not reduce atherosclerosis.

Given *Adamts7* expression in multiple vascular cell types, we next asked if the knockout of *Adamts7* in any single vascular cell type can reduce atherosclerosis. We generated a conditional knockout model of *Adamts7* where exons five and six are floxed (Supplemental Figure 1A). Given the strong prior literature on ADAMTS7 regulation of SMC function, we crossed this mouse to the *Myh11*-CreER^{T2} and *Ldlr*^{KO} to generate a hyperlipidemic SMC conditional knockout of *Adamts7*. (*Adamts7*$^{fl/fl}$; *Ldlr*^{KO}; *Myh11*-CreER^{T2}, referred to as *Adamts7*^{SMCKO} *Ldlr*^{KO}) (Figure 2A). We induced knockout through tamoxifen intraperitoneal

injections one week before WTD initiation. After 16 weeks of WTD feeding, we observed no changes in body weight or total cholesterol (Supplemental Figure 1, B and C). Surprisingly, *Adamts7*^{SMCKO} *Ldlr*^{KO} did not alter the lesion area at either the en-face (Figure 2B) or aortic root levels (Figure 2C). Given the high EC expression of *ADAMTS7* expression in the human scRNAseq, we also crossed the conditional knockout mouse to the *Cdh5*-CreER^{T2} and *Ldlr*^{KO} strains to generate a hyperlipidemic EC conditional knockout of *Adamts7* (*Adamts7*$^{fl/fl}$; *Ldlr*^{KO}; *Cdh5*-CreER^{T2}, referred to as *Adamts7*^{ECKO} *Ldlr*^{KO}). After 16 weeks of WTD feeding, we assessed atherosclerosis in *Adamts7*^{ECKO} *Ldlr*^{KO} compared to controls *Adamts7*^{ECWT} *Ldlr*^{KO} (Figure 2D). Again, we observed no changes in body weight or total cholesterol levels (Supplemental Figure 1, D, and E). Similar to *Adamts7*^{SMCKO} *Ldlr*^{KO} mice, EC knockout of *Adamts7* also did not demonstrate any changes in the atherosclerotic burden relative to controls (Figure 2, E and F). These data strongly suggest that knockout of *Adamts7* in any single vascular cell type is not adequate to alter atherogenesis in mice.

Transgenic overexpression of *Adamts7* in mouse SMCs or ECs exacerbates atherosclerosis.

Given that knockout of *Adamts7* in any single cell type does not reduce atherogenesis, we next asked if induction of *Adamts7* expression in a single cell type can increase atherogenesis. ADAMTS7 is induced in multiple vascular cell types in human atherosclerosis (Figure 1A). We generated a transgenic mouse model with conditional Adamts7 overexpression to mimic its induction and promote its function. We inserted murine *Adamts7* into the Rosa26 locus with a lox-stop-lox (LSL) cassette preceding the gene, allowing for tissue type-specific overexpression of *Adamts7*. The transgenic overexpression model was subsequently bred to the *Ldlr*^{KO} background as well as to either the *Myh11*-CreER^{T2} (*Adamts7*^{SMCTG}) or the *Cdh5*-CreER^{T2} (*Adamts7*^{ECTG}) to allow for SMC (Figure 3A) or EC (Figure 3G) specific overexpression of *Adamts7* respectively. We verified *Adamts7* overexpression in the SMC transgenic model via qPCR (Supplemental Figure 2A) and western blot (Supplemental Figure 2B) from isolated aorta RNA and protein. We note that *Adamts7*^{SMCTG} *Ldlr*^{KO} exhibited a large-fold change in *Adamts7* RNA, but this is partly due to the near complete absence of baseline expression of *Adamts7*. Primary SMC explants from

Adamts7^{SMCTG} displayed increased migration (Supplemental Figure 2C), consistent with prior findings (7). Validation of *Adamts7*^{ECTG} was achieved by examining *Adamts7* expression in isolated CD31+ mouse lung ECs (Supplemental Figure 2D); *Adamts7* expression was elevated in ECs, whereas CD31- cells denoted as non-ECs showed no difference in *Adamts7* expression.

Adamts7 overexpression was induced in all animal models via tamoxifen injection, and mice were fed WTD for 16 weeks. There were no plasma cholesterol or body weight changes in any animal models (Supplemental Figure 3E-H). *Adamts7*^{SMCTG} *Ldlr*^{KO} mice had a stark 3.5-fold increase in atherosclerosis as shown by en-face Oil Red O (ORO) staining as compared to control *Adamts7*^{SMCCTL} *Ldlr*^{KO} mice (Figure 3B) but no change in the aortic root lesion area as assessed by H&E staining (Figure 3C). Given the dramatic increase in aortic atherosclerosis, we asked whether shorter durations of WTD feeding in this model would confer an atherosclerosis phenotype. Indeed, we found increased atherosclerosis at three, six, and nine weeks of WTD feeding (Supplemental Figure 3).

During atherosclerosis, SMCs have an essential role in plaque stabilization (19). As such, we further characterized the aortic root plaque morphology in *Adamts7*^{SMCTG} *Ldlr*^{KO} mice. We found no changes in necrotic core area (Figure 3D) or macrophage content via MAC2 staining (Figure 3E). However, *Adamts7*^{SMCTG} *Ldlr*^{KO} lesions had reduced SMC content as determined by ASMA staining (Figure 3E), especially in the fibrous cap region. The reduction in ASMA also coincided with a 48% reduction in fibrous cap thickness as assessed through picrosirius red staining (Figure 3F). The lack of changes in MAC2 staining and the reduction in cap thickness indicates that SMCs mediate the decrease in plaque stabilization conferred by ADAMTS7.

Finally, in tandem, we performed a similar atherosclerosis study on the *Adamts7*^{ECTG} *Ldlr*^{KO} mice and observed a 1.5-fold increase in aortic atherosclerosis in *Adamts7*^{ECTG} *Ldlr*^{KO} mice as compared to controls

(Figure 3H). We also observed the same lack of aortic root lesion area changes between groups (Figure 3I).

***Adamts7* promotes SMC foam cell formation.**

The significant increase in ORO staining of the en-face aorta indicates an increased accumulation of neutral lipids within vascular cells, presumably due to an expansion in foam cell formation. Thus, we next sought to assess aortic foam cell content in our *Adamts7* transgenic mice using a neutral lipid dye, LipidTOX. After excluding debris, doublets, and dead cells (Supplemental Figure 4), we observed that the *Adamts7*^{SMCTG} *Ldlr*^{KO} had a threefold increase in foam cell content, mirroring the rise in aortic atherosclerosis (Figure 4A). Notably, over 80% of these foam cells lacked CD11B and CD64, indicating that non-leukocytes are accumulating lipids and becoming foamy (Figure 4B) (20).

To further confirm that the increase in foam cells was predominantly of SMC origin, the *Adamts7*^{SMCCTL} *Ldlr*^{KO} and *Adamts7*^{SMCTG} *Ldlr*^{KO} mouse model was subsequently bred to an LSL-ZsGreen reporter to allow for the lineage tracing of SMCs and their derived cells: *Adamts7*^{SMCCTL} *Ldlr*^{KO} ZsGreen^{SMC+} and *Adamts7*^{SMCTG} *Ldlr*^{KO} ZsGreen^{SMC+} (12). Confirmation of efficient ZsGreen labeling of SMCs was achieved through microscopy (Figure 4C). After 12 weeks of WTD feeding, we determined ZsGreen status and concurrently stained with CD45, revealing that over 65% of lipid-laden foam cells were positive for ZsGreen and negative for CD45, indicating again that *Adamts7* was predominately increasing SMC foam cell formation (Figure 4D). We repeated the foam cell analysis within *Adamts7*^{ECCCTL} *Ldlr*^{KO} and *Adamts7*^{ECTG} *Ldlr*^{KO} and observed that the *Adamts7*^{ECTG} *Ldlr*^{KO} mice contained an increase in foam cell content as well (Figure 4E). Further assessment of the foam cells within the aorta revealed that the majority were devoid of CD45 and CD31 while being positive for CD200 (20), indicating that SMCs are also becoming foamy in this model (Figure 4F).

To determine if ADAMTS7 promotes SMC foam cell formation through increased lipid uptake, we generated primary SMC explants from the *Adamts7*^{SMCCTL} and *Adamts7*^{SMCTG} mice and treated them with 10ug/mL of DiI-oxLDL. *Adamts7*^{SMCTG} primary SMCs showed a 38% increase in DiI-oxLDL uptake compared to *Adamts7*^{SMCCTL} as measured by median fluorescence intensity (MFI) (Figure 4G). Notably, the percentage of positive cells and the degree of staining per cell increased within the *Adamts7*^{SMCTG} cells. We corroborated a role for Adamts7 in SMC oxLDL uptake using primary SMCs explanted from our previously described whole-body knockout mice (7). Cells were treated with TNFα for 72 hours to induce *Adamts7* and subsequently loaded with 10ug/mL DiI-oxLDL. Knockout of *Adamts7* reduced the percentage of cells accumulating lipids and the amount of lipid uptake (Figure 4H), complementing the transgenic phenotype.

***Adamts7* leads to an increase in lipid uptake gene expression in SMCs.**

To identify how ADAMTS7 mediates an increase in SMC lipid uptake, we performed bulk RNAseq on SMCs explanted from *Adamts7*^{SMCCTL} and *Adamts7*^{SMCTG} mouse aortas ten days after transgene induction (Figure 5A). Notably, these cells were from mice with wildtype *Ldlr* expression and fed a chow diet, ensuring that any changes in gene expression are due specifically to increased *Adamts7* expression. RNAseq revealed that *Adamts7*^{SMCTG} cells had increased expression of lipid uptake genes typically associated with macrophages, including *Cd36, Fabp5*, and *Trem2,* as well as the macrophage-associated marker *Adgre1*. Follow-up qRT-PCR in whole aorta RNA from *Adamts7*^{SMCTG} mice validated the RNAseq in vivo (Figure 5B). While the increase in macrophage-like gene expression indicates SMC phenotypic modulation, we did not observe decreases in canonical SMC contractile markers within the RNAseq or by qRT-PCR, nor did we observe any changes in *Klf4* expression, a marker typically associated with modulated SMCs (Supplemental Figure 5A) (13). Ingenuity Pathway Analysis (IPA) on the differentially expressed gene set identified pathways enriched within the *Adamts7*^{SMCTG} SMCs typically ascribed to macrophages, such as phagosome formation and immune signaling (Figure 5C). As one of the hallmark functions of macrophages during atherosclerosis is perpetuating inflammation, we

asked whether our *Adamts7*^{SMCTG} SMCs were more inflammatory. Assaying the conditioned media of these SMCs did not demonstrate differences in IL1β, IL18, IL6, or TNFα cytokine secretion (Supplemental Figure 5B), indicating that these SMCs are not proinflammatory and any atherosclerosis phenotype is independent of these canonical inflammatory pathways. Overall, the RNAseq and qRT-PCR data indicate that *Adamts7*^{SMCTG} SMCs acquire a gene signature typically associated with macrophages, with an enrichment of phagocytic and lipid-uptake genes, consistent with prior reports that SMCs can upregulate macrophage processes when lipid-loaded (21).

Knockdown of *Cd36* ameliorates enhanced oxLDL uptake conferred by *Adamts7*.

Given the known role of CD36 as a receptor for oxLDL (22), we further investigated its role in mediating the increased lipid uptake observed in *Adamts7*^{SMCTG} cells. We corroborated the increase in CD36 in vivo using flow cytometry on cells from digested *Adamts7*^{SMCTG} *Ldlr*^{KO} ZsGreen^{SMC+} aortas after 12 weeks of WTD feeding. ZsGreen+ cells from *Adamts7*^{SMCTG} *Ldlr*^{KO} ZsGreen^{SMC+} mice had a 40% increase in cells expressing *Cd36* and a 2.3-fold increase in MFI of CD36 signal (Figure 5D), consistent with the in vitro increase in CD36 expression in *Adamts7*^{SMCTG} cells. Next, we tested whether CD36 was mechanistically responsible for increased oxLDL uptake in *Adamts7*^{SMCTG} cells. siRNA-mediated knockdown of *Cd36* in primary SMCs from *Adamts7*^{SMCCTL} and *Adamts7*^{SMCTG} mice reduced *Cd36* expression to that of Non-Targeting Control (NTC) treated *Adamts7*^{SMCCTL} cells (Figure 6A). We next assessed oxLDL uptake and found that treatment of *Adamts7*^{SMCTG} cells with si*Cd36* reduced oxLDL uptake levels to that of NTC-treated *Adamts7*^{SMCCTL} cells, in agreement with the observed *Cd36* RNA levels (Figure 6B). These findings confirm a role for *Cd36* in mediating the increase in oxLDL uptake and subsequent SMC foam cell formation caused by *Adamts7* during atherosclerosis.

Knockdown of Spi1 in *Adamts7* overexpressing SMCs attenuates the expression of macrophage-like and lipid-uptake genes.

We used IPA to identify upstream transcriptional regulators that could mediate the observed differential gene expression (Table 1) in *Adamts7*^{SMCTG} cells. The top predicted activated transcription factor was *Spi1,* which encodes the protein PU.1. *Spi1* itself also exhibited a 3.16-fold increase in expression in *Adamts7*^{SMCTG} cells. To test whether PU.1 is required for the *Adamts7*-mediated increase in lipid uptake genes, we used siRNA to achieve 66% knockdown *Spi1* in primary SMCs. Knockdown of *Spi1* abrogated the increases in gene expression of *Cd36, Fabp5*, *Trem2, Adgre1*, and *Cd68* (Figure 6C). We also performed siRNA knockdown of other predicted master regulator transcription factors identified by IPA and found that knockdown of *Cebpa*, *Smarca4*, *Bhlhe40*, and *Klf6* did not ameliorate the increases in lipid uptake gene expression (Supplemental Figure 6), excluding a role for these transcription factors. Finally, DiI-oxLDL loading of primary *Adamts7*^{SMCTG} SMCs with *Spi1* knockdown demonstrated that loss of *Spi1* attenuated the increased oxLDL uptake in *Adamts7*^{SMCTG} cells while having no effect in *Adamts7*^{SMCCTL} primary SMCs (Figure 6D). This finding indicates that increased PU.1 levels caused by *Adamts7* expression are responsible for the increased oxLDL uptake observed in *Adamts7*^{SMCTG} SMCs. Finally, we examined the level of *SPI1* expression within our human single-cell data and found clear *SPI1* expression within the modulated SMC populations (Figure 6E), consistent with our observations in mice.

DISCUSSION

GWAS have revealed over 300 genomic regions associated with CAD (2, 23). However, functional studies to elucidate the precise mechanisms of these targets are still in their infancy, hampering the clinical translation of these genetic findings. In 2011, our group and others reported *ADAMTS7* as a GWAS gene for CAD (4). Subsequent GWAS studies have replicated this signal multiple times and across different ethnic groups (2, 23), highlighting the importance of ADAMTS7 in CAD pathogenesis. Further studies in mice demonstrated that ADAMTS7 is proatherogenic and that its atherogenicity is conferred from its catalytic function (7, 9). Despite the large body of prior work on ADAMTS7, more is needed to understand how ADAMTS7 participates in atherogenesis. Additionally, there have yet to be

any cell-specific in vivo ADAMTS7 studies, leaving the question of which vascular cell type(s) is critical for ADAMTS7 function. Here, we identified prominent expression of ADAMTS7 in human and mouse endothelial and stromal cells and developed multiple novel mouse models in which *Adamts7* can be genetically overexpressed or conditionally knocked out in a cell-specific manner. Through these models, we demonstrate that both SMC- and EC-derived expression of *Adamts7 can* be proatherogenic, while knockout of *Adamts7* in either cell type alone is not sufficient to alter atherogenesis. Our findings suggest redundant pro-atherogenic effects of ADAMTS7 derived from different cell types mediated through a common mechanism involving SMC foam cells: ADAMTS7 promotes SMC foam cell formation via increased oxLDL uptake due to increased expression of *Spi1* and the *Spi1* target *Cd36*.

Adamts7 has very low overall expression across all murine vascular cell types in the basal state, and its expression is induced in response to vascular injury such as endothelial denudation or prolonged hyperlipidemia (7, 15). In primary mouse aortic SMCs, *Adamts7* induction is required to confer a detectable migration phenotype (7), confirming that this induction is critical for ADAMTS7 function. At terminal time points in mouse atherosclerosis studies, *Adamts7* is again undetectable in plaques (7, 9), suggesting that *Adamts7* induction is transient and ADAMTS7 is mechanistically active in mice during plaque maturation. The transient induction of *Adamts7* has made studying its exact function in vascular cells difficult. The novel *Adamts7* mouse models presented here help to overcome this obstacle, demonstrating that prolonged expression of *Adamts7* in either SMCs or ECs can drive atherosclerosis progression.

While neither *Adamts7*^{SMCKO} *Ldlr*^{KO} nor *Adamts7*^{ECKO} *Ldlr*^{KO} affected atherosclerosis, prior research on whole-body knockout models indicates that *Adamts7* is pro-atherogenic. These prior published studies include three unique models of whole-body *Adamts7* inactivation. Two models employed genetic perturbation to inactivate ADAMTS7 by either exon deletion or mutation of the ADAMTS7 catalytic site (7, 9). The third approach is to vaccinate against ADAMTS7 (10). While prior findings clearly demonstrate

that *Adamts7* is expressed in cultured SMCs (7, 9, 15, 24), our RNAscope studies of *Adamts7* expression revealed its induction in multiple vascular cell types during murine atherosclerosis while also demonstrating how few vascular cells actually express *Adamts7*. These observations imply that no specific cell type is exclusively responsible for the proatherogenic effects of ADAMTS7. This could be because there is either redundant Adamts7 expression from multiple vascular cell types or the contribution to atherogenesis of each individual cell type alone is negligible. Whether ADAMTS7, a secreted protein, acts exclusively in a cell-autonomous manner or across multiple plaque cell types remains an unanswered question.

Exactly how these findings translate to human atherosclerosis is another open question. Our analysis of the most extensive carotid plaque single-cell data set to date highlights that ECs and SMCs both express *ADAMTS7*, aligning with the results of our mouse studies. This scRNAseq data also shows that mast cells and fibroblasts have detectable *ADAMTS7* expression, highlighting these cell types for further ADAMTS7 studies. Notably, the scRNAseq data comes from mature atherosclerotic plaques, while our mouse data suggests the window for ADAMTS7 activity is earlier in plaque progression. Thus, whether this human expression pattern reflects relevant ADAMTS7 activity remains to be determined. Additionally, the effectiveness of targeting ADAMTS7 function in a mature plaque is unknown. Nonetheless, these human data demonstrate that ADAMTS7 is active in multiple vascular cell types, and our mouse data shows that sustained ADAMTS7 activity in any individual cell type can drive atherogenesis.

Our SMC-specific and EC-specific Adamts7 overexpression mouse models have increased atherosclerotic burden and aortic foam cell formation. We also note that these foam cells are SMC-derived. Although macrophages have historically been thought to be the source of foam cells in atherosclerotic lesions, it is increasingly appreciated that SMCs constitute most foam cells in atherosclerosis (14). When *Adamts7* is induced in the vasculature, SMCs increase their expression of genes involved in lipid uptake, inflammation, and phagocytosis, a gene expression profile reminiscent of

a macrophage. Recent studies have definitively shown that SMCs do not contribute to the pool of mature macrophages in atherosclerosis (25). Thus, we posit that these *Adamts7*^{SMCTG} SMCs are modulated SMCs with increased lipid uptake capacity and foam cell features. While the specific role of SMC foam cells in atherosclerosis remains unclear, it has been reported that SMC foam cells and true macrophages differ in their intracellular lipid metabolism (26, 27). Lipid-laden, foamy macrophages tend to be less inflammatory (28), and by becoming foamy, these macrophages may no longer contribute to the inflammatory cycle associated with atherosclerosis, raising the possibility that foamy macrophages are beneficial in atherosclerosis. Conversely, we observed reduced fibrous cap thickness with *Adamts7* overexpression. As one well-described role of SMCs is forming the fibrous cap, it is possible that foamy SMCs cannot stabilize lesions, raising an intriguing possibility that macrophage foam cells are beneficial, whereas SMC foam cells are detrimental. In Sharifi et al., the authors showed that ADAMTS7 degrades TIMP1, increasing MMP2 and MMP9 activity (29). Consistent with that model, ADAMTS7 whole-body knockout increased collagen content and plaque stabilization, and *ADAMTS7* expression was found to be higher in caps of unstable human carotid plaques (29). These findings and those presented here support the adverse role of ADAMTS7 in plaque stability and suggest multiple mechanistic explanations for ADAMTS7-mediated plaque instability.

Mechanistically, we chose to pursue the function of SMC *Adamts7* given the large body of preexisting data on *Adamts7* modulation of SMC function. We find that constitutive *Adamts7* SMC expression drives significant changes in lipid uptake gene expression, leading to increased SMC oxLDL uptake. Of these lipid uptake genes, one of the most significantly upregulated genes was *Cd36*. CD36 is a well-described receptor for oxLDL, and our studies demonstrate that CD36 is mainly responsible for the SMC foam cell phenotype in *Adamts7*^{SMCTG} mice (22). In addition, upstream regulator analysis of primary SMCs indicates that *Spi1* is significantly upregulated (30), and knockdown of *Spi1* in SMCs ameliorates the increase in lipid handling gene expression and macrophage markers. *Spi1*, which codes for the PU.1 transcription factor, is long recognized as a critical mediator of hematopoietic lineage commitment. These observations

suggest that PU.1 may also be a crucial factor in driving the production of foamy SMCs in vivo. Thus, future cell-specific studies of SMC PU.1 may help reveal disease-relevant consequences of foamy SMCs. A critical remaining knowledge gap is the mechanism by which ADAMTS7, a secreted factor, upregulates the SMC expression of *Spi1*. The proatherogenicity of ADAMTS7 is conferred by its catalytic activity (9); thus, the cleavage of some extracellular substrate by ADAMTS7 may lead to outside-in signaling and downstream induction of *Spi1*. ADAMTS7 substrates have been proposed in prior studies (8, 29, 31, 32), but none have been tested in the context of SMC foam cell formation, and the precise cleavage substrate mediating ADAMTS7 proatherogenicity remains elusive.

In conclusion, our investigation using novel mouse models revealed that ADAMTS7 promotes SMC foam cell formation and atherosclerosis while reducing plaque stability. Our mechanistic studies show that ADAMTS7 stimulates SMCs to uptake lipids in a process dependent on PU.1 and CD36. Our conditional knockout model revealed that the proatherogenicity conferred by ADAMTS7 is not due to any singular vascular cell type. Via the integration of carotid atherosclerosis scRNAseq and RNAscope within atherosclerotic mice, we have identified that ECs are an alternative source of ADAMTS7 in the vasculature. These studies elucidate novel mechanisms governing ADAMTS7 proatherogenicity and link human GWAS to emerging research on SMC foam cells.

Author Contributions

AC led the study and was directly involved in most experiments. HKC, KS, CVM, and JG conducted experiments and acquired data. HP helped generate mouse lines. ACB, HY, and ML provided human single-cell data. RCB oversaw the design, execution, management, and funding of all studies. AC and RCB wrote the manuscript, which all authors approved before submission.

Acknowledgments

AC is supported by an American Heart Association Predoctoral Fellowship (909206). HP is supported by National Institute of Health (NIH) grants 5K99HL153939 and R00HL153939. ACB is supported by the NIH Postdoctoral Training in Arteriosclerosis fellowship 5T32HL007343. KS is supported by NIH Training in Cellular, Molecular and Biomedical Studies 5T32GM145766. ML is supported by NIH grants R01GM125301, R01HL113147, R01HL150359, and R21HL156234. RCB is supported for this work by NIH grants R01HL141745 and R01DK134026.

We want to thank Dr. Muredach P. Reilly for guidance in executing these studies. We thank the staff of the Columbia Stem Cell Initiative Flow Cytometry Core Facility, under the leadership of Michael Kissner at Columbia University Irving Medical Center, for their contributions to the work presented in this manuscript. We also thank Dr. Carol Troy for providing the *Cdh5*-CreER^{T2} mice.

METHODS

Sex as a biological variable

Our human data contained both male and female samples. SMC mouse studies were limited to male mice due to the integration of the *Myh11*-CreER^{T2} onto the Y-chromosome.

Animals

C57BL/6J (Stock:000664), *Ldlr*^{KO} (Stock: 002207), ZsGreen (Stock: 007906), and *Myh11*-CreER^{T2} (Stock: 019079) were purchased from the Jackson Laboratory and bred in our laboratory. *Adamts7* knockout mice were previously described (7). The *Cdh5*-CreER^{T2} Mouse was developed by the laboratory of Ralf Adams and has been previously described (33). To generate a floxed *Adamts7*, the *Adamts7* knockout mouse (MMRRC:046487) was bred to an FLP recombinase mouse. *Adamts7* transgenic mice were created by cloning the mouse allele of *Adamts7* into the pR26 CAG/GFP Asc plasmid (Addgene plasmid # 74285). Subsequently, FL19 embryonic stem cells were used to generate chimeras, which

were then crossed to the C57BL/6J background. For CreER^{T2} activation, tamoxifen (Sigma-Aldrich: T5648) was dissolved in 90% corn oil and 10% ethanol; subsequently, mice at seven weeks of age were injected with tamoxifen for five days at a dosage of 40mg/kg of body weight per day. At eight weeks of age, the mice were fed a WTD consisting of 40% Kcal by fat and 0.15% Cholesterol (Research Diet: D12079Bi). For blood collection, mice were fasted for four hours and subsequently sedated with isoflurane, and blood was collected by retroorbital puncture with heparinized microcapillary tubes. Plasma was isolated by centrifugation at 1500 RCF for 10 minutes at 4C. Total cholesterol was measured using the Infinity Cholesterol Reagent (Thermo Scientific: R22421).

Atherosclerosis analysis

For atherosclerosis studies, mice were sacrificed by cervical dislocation and perfused with PBS. The aorta was dissected and subsequently fixed in 10% formalin. Whole aortas were stained with ORO. Hearts containing the aortic root were fixed in 4% paraformaldehyde for 24 hours, transferred to 70% ethanol, and embedded in paraffin wax. Sectioning was performed using a Leica microtome at 8um thickness. The heart was sectioned from the inferior heart towards the aortic root. 25 slides were collected, with each slide containing two sections. We aimed to have the breakage of the leaflet occur on slide 13. Slides 3, 8,13,18, and 23 were used for hematoxylin and eosin staining to allow for lesion size quantification using ImageJ. Hematoxylin and Eosin, and Picrosirius Red staining was performed at Columbia's Molecular Pathology Shared Resource.

Immunofluorescence

Immunofluorescence was performed on paraffin sections of the aortic root. Deparaffinization was performed using xylene. Antigen retrieval was performed using a citrate-based agent. Sections were subsequently blocked using 10% normal goat serum for at least one hour. Subsequently, the sections were stained using the following antibodies and dilutions 1:1000 ASMA-Cy3 (Sigma Aldrich: C6198), 1:500 MAC2. IgG controls were purchased from Jackson Immunoresearch. The sections were washed

with PBS containing 0.01% Tween 20. For the secondary antibody, a donkey anti-rabbit Alexa Fluor 647 (Invitrogen: A-31573) and goat anti-mouse Alexa Fluor 546 (Invitrogen: A-11030) were used, both at a 1:1000 dilution in 1% goat serum. The slides were washed and mounted with ProLong Glass Antifade Mountant with NucBlue Stain. Imaging was conducted on a Nikon Eclipse Ti-S microscope, and image processing was performed using ImageJ.

Vascular SMC isolation for tissue culture

SMC isolation was isolated as previously described (34). The aorta was dissected from the ascending arch to the diaphragm and was predigested for 10 minutes at 37°C with 175U/ml Collagenase II and 1.25U/ml elastase in HBSS to allow for the removal of the adventitia. After removing the adventitia, the media layer was further digested in 400U/ml collagenase II, 2.5U/ml elastase, and 0.2mg/ml soybean trypsin inhibitor at 37°C for one hour in a rotating incubator. The cells were cultured in DMEM supplemented with 20% fetal bovine serum, 1% L-Glutamine, 1% sodium pyruvate, and 1% Penicillin Streptomycin. Cells between passages two and seven were used for experiments.

Vascular SMC isolation for flow analysis

Mice were sacrificed and perfused with PBS. The ascending aorta to the bifurcation at the common iliac artery was dissected and digested with a cocktail consisting of 4 U/mL Liberase TM (Sigma-Aldrich: 5401127001), 60 U/mL hyaluronidase (Sigma-Aldrich: H3506), and 60 U/mL DNase I (Worthington Biochemical Corporation: LS006333) in RPMI-1640. The digestion enzymes were neutralized with 10% FBS in RPMI and washed once in FACS buffer (2% FBS, 5 mM EDTA, 20 mM HEPES, and 1 mM Sodium Pyruvate in DPBS). Cells were then blocked with TruStain FcX PLUS (anti-mouse CD16/32) (Biolegend: 156603) for 10 mins at 4°C. Staining was performed in FACS buffer at the following dilutions: 1:1000 LipidTox Red (Thermo Scientific: H34476), 1:100 CD36 Super Bright 600 (Invitrogen: 63-0362-82), 1:200 CD45-Alexafluor700 (Biolegend: 157209). Cell viability was assessed with DAPI. To establish the

LipidTOX high population and thus foamy cells, a C57BL6J mouse with normal lipidemia was used as previously described (14).

In vitro cell culture experiments

For in vitro foam cell analysis, cells were treated with Dil conjugated oxLDL (Invitrogen: L34358) at a concentration of 10ug/mL for 24 hours. Subsequently, they were washed with PBS and detached using 0.25% Trypsin EDTA. Neutralization of trypsin was performed using FACS buffer. The cells were counterstained with DAPI to assess live cells, and all analysis was done using either a Novocyte Quanteon or Penteon. For siRNA experiments, all siRNAs were purchased from IDT. Transfection was performed using RNAimax according to the manufacturer's protocol. All siRNAs were used at a concentration of 10nM.

RNA Isolation and quantitative RT-PCR

For tissue samples, specimens were collected in Trizol, and homogenization was performed using a tissue lyser (Qiagen). The RNA was extracted using the Direct-zol RNA MiniPrep Kit (Zymo) according to the manufacturer's instructions. For cells, RNA was collected using the Quick-RNA Microprep Kit (Zymo). Complementary DNA was synthesized using High-Capacity cDNA Reverse Transcription Kit (Applied Biosystem). All qPCR was performed using TaqMan probes and performed on the Applied Biosystems QuantStudio 7 Flex Real-Time PCR System. Analysis was performed using the 2-DCCT Method.

RNAscope

RNAscope was performed on sections of mouse BCAs after specified durations of WTD feeding. The BCAs were freshly frozen and sectioned at 8um thickness. Human coronary arteries were paraffin embedded. RNAscope was performed according to the manufacturer's instructions. The sections were first fixed in 10% neutral buffered formalin. Subsequently, the sections were dehydrated and treated with

hydrogen peroxide and protease. Hybridization with *Adamts7* (Advanced Cell Diagnostics: 533341) and *Pecam1* (Advanced Cell Diagnostics: 316721-C3) probes was performed. After probe hybridization, hybridization with AMPs 1-3 was performed. Signal development was conducted using Akoya Biosciences Opal Reagent Kits, and slides were mounted using Prolong Glass Antifade Mountant (Thermo Scientific: P36984). Imaging was conducted on a Nikon Eclipse Ti-S microscope, and image processing was performed using ImageJ.

Western blot

Samples were lysed in RIPA buffer (Thermo Scientific) supplemented with 1% Halt Protease and Phosphatase Inhibitor Cocktail. Tissue samples were lysed with the Qiagen TissueLyser and samples were subsequently cleared by centrifugation at 20,000 RCF for 10 minutes at 4C. Samples were denatured, resolved on a 4-12% Bis-Tris gel, and transferred to either PVDF or a nitrocellulose membrane. Blocking was performed with 5% milk, and primary antibodies were diluted 1:1000 in 5% milk and incubated overnight at 4C. Membranes were washed with 0.1% TBST and probed with the appropriate secondary antibody for one hour at room temperature. Membranes were visualized with ECL using the Amersham Imager 600 gel imager.

Statistics

All statistical tests are indicated in figure legends. P values were calculated using a 2-tailed Student's t-test in GraphPad Prism 10. $P < 0.05$ was considered significant. ANOVA analysis with multiple corrections was used for comparison between groups with Sidak's post-analysis as indicated in the figure legends. Aortic root histology, qPCR, and ELISA results are presented as mean ± standard error of the mean. All other data is presented as mean ± standard deviation.

Study approval

All mouse experiments were performed according to procedures approved by Columbia University's Institute for Animal Care and Use Committee under protocol AABU8650. The Institutional Review Board of Columbia University approved all human studies under IRB AAAJ2765 and AAAR6796 with written informed consent provided by all participants.

Data availability

Human carotid artery scRNAseq has been previously published (18). RNAseq data has been deposited in the NCBI's Gene Expression Omnibus database (GEO XXXX)

REFERENCE

1. Tsao CW, Aday AW, Almarzooq ZI, Anderson CAM, Arora P, Avery CL, et al. Heart Disease and Stroke Statistics-2023 Update: A Report From the American Heart Association. *Circulation.* 2023.
2. Aragam KG, Jiang T, Goel A, Kanoni S, Wolford BN, Atri DS, et al. Discovery and systematic characterization of risk variants and genes for coronary artery disease in over a million participants. *Nat Genet.* 2022;54(12):1803-15.
3. Nikpay M, Goel A, Won HH, Hall LM, Willenborg C, Kanoni S, et al. A comprehensive 1,000 Genomes-based genome-wide association meta-analysis of coronary artery disease. *Nat Genet.* 2015;47(10):1121-30.
4. Reilly MP, Li M, He J, Ferguson JF, Stylianou IM, Mehta NN, et al. Identification of ADAMTS7 as a novel locus for coronary atherosclerosis and association of ABO with myocardial infarction in the presence of coronary atherosclerosis: two genome-wide association studies. *Lancet.* 2011;377(9763):383-92.
5. Schunkert H, Konig IR, Kathiresan S, Reilly MP, Assimes TL, Holm H, et al. Large-scale association analysis identifies 13 new susceptibility loci for coronary artery disease. *Nat Genet.* 2011;43(4):333-8.

6. Luan Y, Kong L, Howell DR, Ilalov K, Fajardo M, Bai XH, et al. Inhibition of ADAMTS-7 and ADAMTS-12 degradation of cartilage oligomeric matrix protein by alpha-2-macroglobulin. *Osteoarthritis Cartilage.* 2008;16(11):1413-20.

7. Bauer RC, Tohyama J, Cui J, Cheng L, Yang J, Zhang X, et al. Knockout of Adamts7, a novel coronary artery disease locus in humans, reduces atherosclerosis in mice. *Circulation.* 2015;131(13):1202-13.

8. Chung A, Reilly MP, and Bauer RC. ADAMTS7: a Novel Therapeutic Target in Atherosclerosis. *Curr Atheroscler Rep.* 2023;25(8):447-55.

9. Mizoguchi T, MacDonald BT, Bhandary B, Popp NR, Laprise D, Arduini A, et al. Coronary Disease Association With ADAMTS7 Is Due to Protease Activity. *Circ Res.* 2021;129(4):458-70.

10. Ma Z, Mao C, Chen X, Yang S, Qiu Z, Yu B, et al. Peptide Vaccine Against ADAMTS-7 Ameliorates Atherosclerosis and Postinjury Neointima Hyperplasia. *Circulation.* 2022.

11. Miano JM, Fisher EA, and Majesky MW. Fate and State of Vascular Smooth Muscle Cells in Atherosclerosis. *Circulation.* 2021;143(21):2110-6.

12. Pan H, Xue C, Auerbach BJ, Fan J, Bashore AC, Cui J, et al. Single-Cell Genomics Reveals a Novel Cell State During Smooth Muscle Cell Phenotypic Switching and Potential Therapeutic Targets for Atherosclerosis in Mouse and Human. *Circulation.* 2020;142(21):2060-75.

13. Shankman LS, Gomez D, Cherepanova OA, Salmon M, Alencar GF, Haskins RM, et al. KLF4-dependent phenotypic modulation of smooth muscle cells has a key role in atherosclerotic plaque pathogenesis. *Nat Med.* 2015;21(6):628-37.

14. Wang Y, Dubland JA, Allahverdian S, Asonye E, Sahin B, Jaw JE, et al. Smooth Muscle Cells Contribute the Majority of Foam Cells in ApoE (Apolipoprotein E)-Deficient Mouse Atherosclerosis. *Arterioscler Thromb Vasc Biol.* 2019;39(5):876-87.

15. Wang L, Zheng J, Bai X, Liu B, Liu CJ, Xu Q, et al. ADAMTS-7 mediates vascular smooth muscle cell migration and neointima formation in balloon-injured rat arteries. *Circ Res.* 2009;104(5):688-98.

16. Santamaria S, and de Groot R. ADAMTS proteases in cardiovascular physiology and disease. *Open Biol.* 2020;10(12):200333.

17. Kessler T, Zhang L, Liu Z, Yin X, Huang Y, Wang Y, et al. ADAMTS-7 inhibits re-endothelialization of injured arteries and promotes vascular remodeling through cleavage of thrombospondin-1. *Circulation.* 2015;131(13):1191-201.

18. Bashore AC, Yan H, Xue C, Zhu LY, Kim E, Mawson T, et al. High-Dimensional Single-Cell Multimodal Landscape of Human Carotid Atherosclerosis. *medRxiv.* 2023.

19. Allahverdian S, Chaabane C, Boukais K, Francis GA, and Bochaton-Piallat ML. Smooth muscle cell fate and plasticity in atherosclerosis. *Cardiovasc Res.* 2018;114(4):540-50.

20. Bashore AC, Chung A, Ibikunle C, Yan H, Xue C, Li M, et al. Single-Cell Multimodal Profiling of Atherosclerosis Identifies CD200 as a Cell Surface Lineage Marker of Vascular Smooth Muscle Cells and Their Derived Cells. *Circulation.* 2024;149(15):1231-3.

21. Chattopadhyay A, Kwartler CS, Kaw K, Li Y, Kaw A, Chen J, et al. Cholesterol-Induced Phenotypic Modulation of Smooth Muscle Cells to Macrophage/Fibroblast-like Cells Is Driven by an Unfolded Protein Response. *Arterioscler Thromb Vasc Biol.* 2021;41(1):302-16.

22. Jay AG, Chen AN, Paz MA, Hung JP, and Hamilton JA. CD36 binds oxidized low density lipoprotein (LDL) in a mechanism dependent upon fatty acid binding. *J Biol Chem.* 2015;290(8):4590-603.

23. Tcheandjieu C, Zhu X, Hilliard AT, Clarke SL, Napolioni V, Ma S, et al. Large-scale genome-wide association study of coronary artery disease in genetically diverse populations. *Nat Med.* 2022;28(8):1679-92.

24. Pu X, Xiao Q, Kiechl S, Chan K, Ng FL, Gor S, et al. ADAMTS7 cleavage and vascular smooth muscle cell migration is affected by a coronary-artery-disease-associated variant. *Am J Hum Genet.* 2013;92(3):366-74.

25. Sharma D, Worssam MD, Pedroza AJ, Dalal AR, Alemany H, Kim HJ, et al. Comprehensive Integration of Multiple Single-Cell Transcriptomic Data Sets Defines Distinct Cell Populations

and Their Phenotypic Changes in Murine Atherosclerosis. *Arterioscler Thromb Vasc Biol.* 2024;44(2):391-408.

26. Dubland JA, Allahverdian S, Besler KJ, Ortega C, Wang Y, Pryma CS, et al. Low LAL (Lysosomal Acid Lipase) Expression by Smooth Muscle Cells Relative to Macrophages as a Mechanism for Arterial Foam Cell Formation. *Arterioscler Thromb Vasc Biol.* 2021;41(6):e354-e68.

27. Miller CL, and Zhang H. Clarifying the Distinct Roles of Smooth Muscle Cell-Derived Versus Macrophage Foam Cells and the Implications in Atherosclerosis. *Arterioscler Thromb Vasc Biol.* 2021;41(6):2035-7.

28. Kim K, Shim D, Lee JS, Zaitsev K, Williams JW, Kim KW, et al. Transcriptome Analysis Reveals Nonfoamy Rather Than Foamy Plaque Macrophages Are Proinflammatory in Atherosclerotic Murine Models. *Circ Res.* 2018;123(10):1127-42.

29. Sharifi MA, Wierer M, Dang TA, Milic J, Moggio A, Sachs N, et al. ADAMTS-7 Modulates Atherosclerotic Plaque Formation by Degradation of TIMP-1. *Circ Res.* 2023;133(8):674-86.

30. Inaba T, Gotoda T, Ishibashi S, Harada K, Ohsuga JI, Ohashi K, et al. Transcription factor PU.1 mediates induction of c-fms in vascular smooth muscle cells: a mechanism for phenotypic change to phagocytic cells. *Mol Cell Biol.* 1996;16(5):2264-73.

31. MacDonald BT, Keshishian H, Mundorff CC, Arduini A, Lai D, Bendinelli K, et al. TAILS Identifies Candidate Substrates and Biomarkers of ADAMTS7, a Therapeutic Protease Target in Coronary Artery Disease. *Mol Cell Proteomics.* 2022;21(4):100223.

32. Colige A, Monseur C, Crawley JTB, Santamaria S, and de Groot R. Proteomic discovery of substrates of the cardiovascular protease ADAMTS7. *J Biol Chem.* 2019;294(20):8037-45.

33. Sorensen I, Adams RH, and Gossler A. DLL1-mediated Notch activation regulates endothelial identity in mouse fetal arteries. *Blood.* 2009;113(22):5680-8.

34. Ostriker AC, Xie Y, Chakraborty R, Sizer AJ, Bai Y, Ding M, et al. TET2 Protects Against Vascular Smooth Muscle Cell Apoptosis and Intimal Thickening in Transplant Vasculopathy. *Circulation.* 2021;144(6):455-70.

FIGURE 1

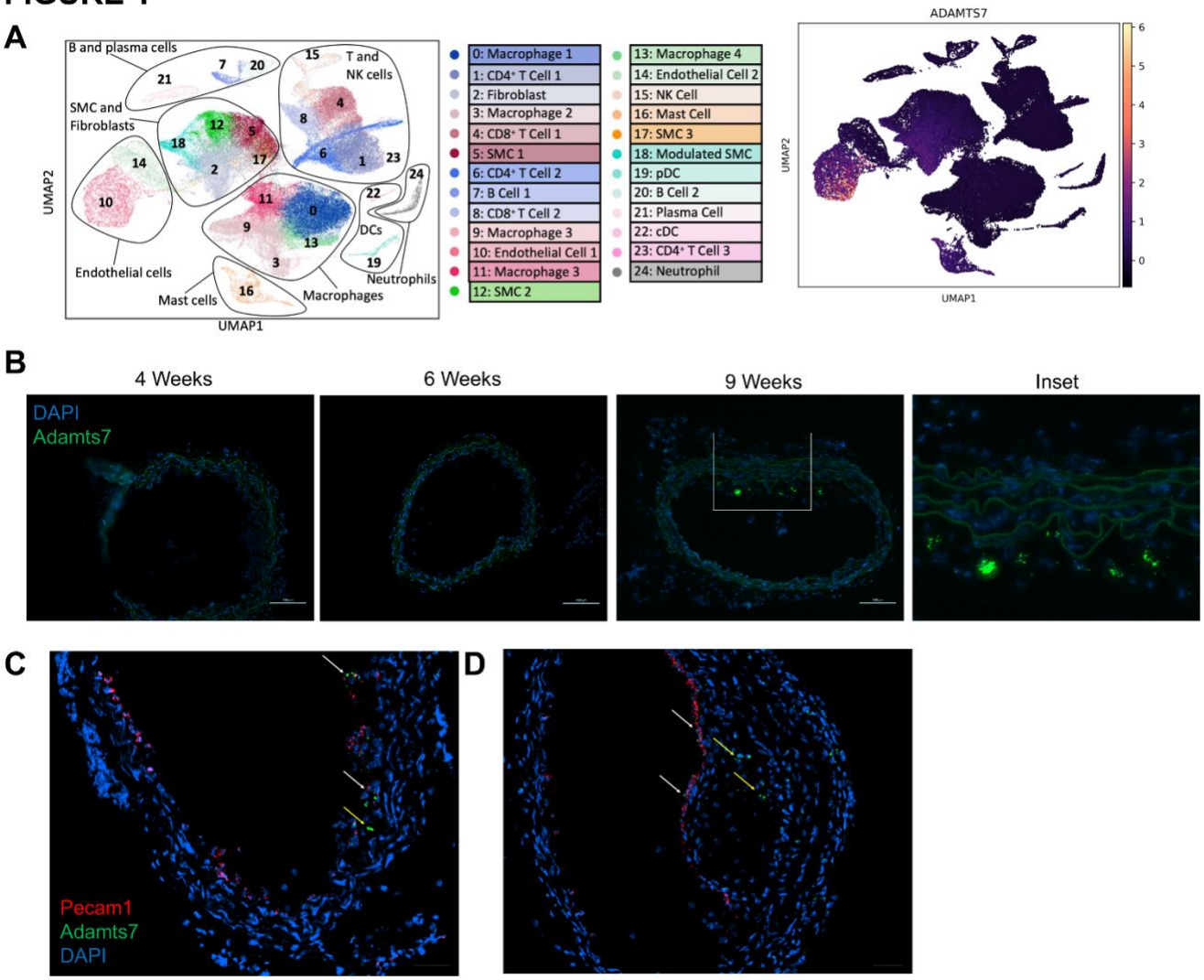
A
B and plasma cells
T and NK cells
SMC and Fibroblasts
Endothelial cells
Mast cells
Macrophages
Neutrophils
DCs
UMAP1
UMAP2
0: Macrophage 1
1: CD4⁺ T Cell 1
2: Fibroblast
3: Macrophage 2
4: CD8⁺ T Cell 1
5: SMC 1
6: CD4⁺ T Cell 2
7: B Cell 1
8: CD8⁺ T Cell 2
9: Macrophage 3
10: Endothelial Cell 1
11: Macrophage 3
12: SMC 2
13: Macrophage 4
14: Endothelial Cell 2
15: NK Cell
16: Mast Cell
17: SMC 3
18: Modulated SMC
19: pDC
20: B Cell 2
21: Plasma Cell
22: cDC
23: CD4⁺ T Cell 3
24: Neutrophil
ADAMTS7
B
4 Weeks
6 Weeks
9 Weeks
Inset
DAPI
Adamts7
C
D
Pecam1
Adamts7
DAPI

Figure 1. Identifying endogenous ADAMTS7 expression. (A) Single Cell RNA sequencing of human carotid atherosclerosis and cell clustering identities. (B) RNAscope of the brachial cephalic artery in mice after WTD feeding. Nuclei are stained with DAPI. Scale bar = 100um. RNAscope of the brachial cephalic artery of *Ldlr*^{KO} mice after seven (C) and ten (D) weeks of WTD feeding and probed against *Adamts7* and *Pecam1*. White arrows highlight EC expression of *Adamts7*. Yellow arrows indicate non-EC expression of *Adamts7*. Scale bar = 50um.

FIGURE 2

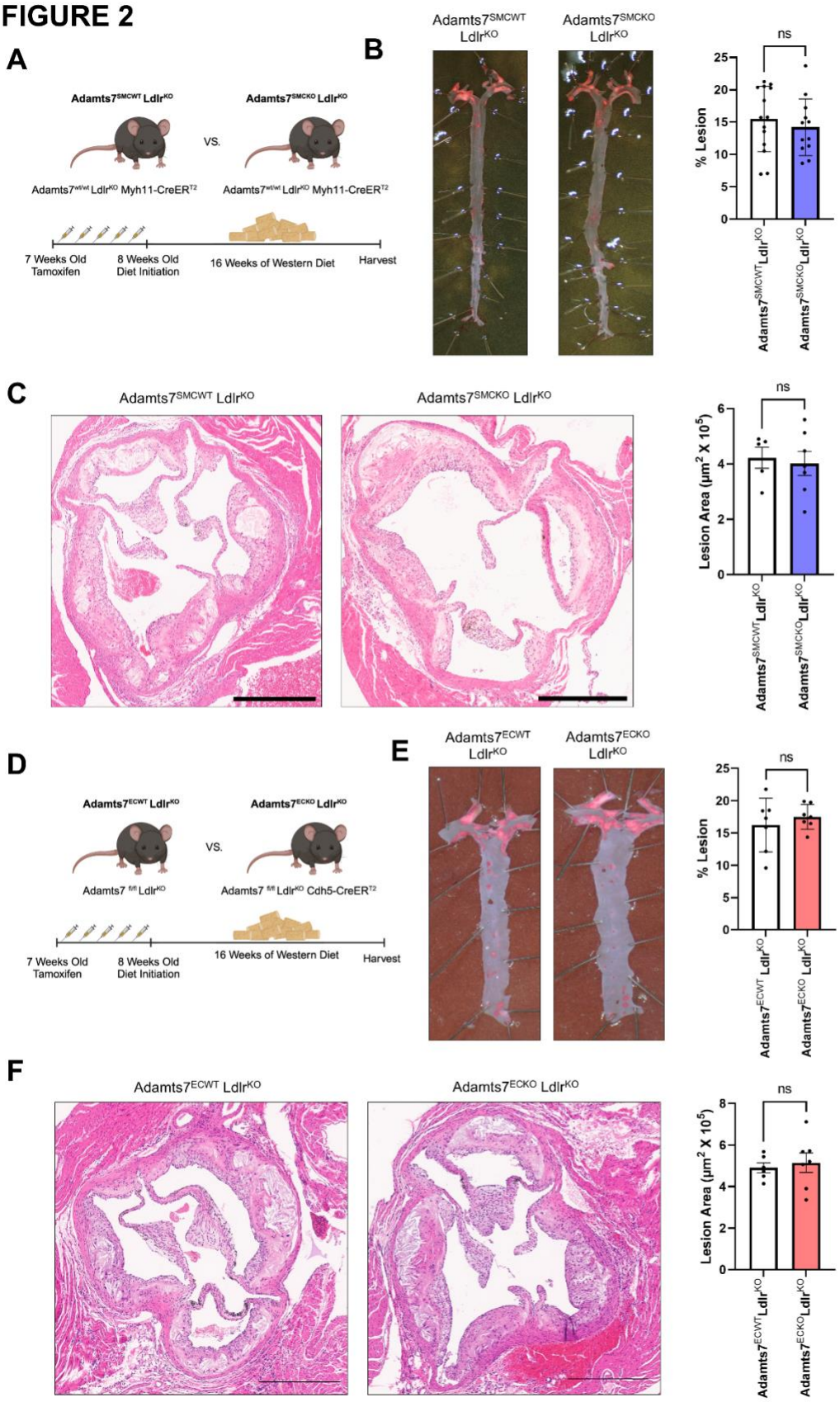
A
Adamts7SMCWT LdlrKO
VS.
Adamts7SMCKO LdlrKO
Adamts7wt/wt LdlrKO Myh11-CreERT2
Adamts7wt/wt LdlrKO Myh11-CreERT2
7 Weeks Old Tamoxifen
8 Weeks Old Diet Initiation
16 Weeks of Western Diet
Harvest
B
Adamts7SMCWT LdlrKO
Adamts7SMCKO LdlrKO
ns
% Lesion
Adamts7SMCWT LdlrKO
Adamts7SMCKO LdlrKO
C
Adamts7SMCWT LdlrKO
Adamts7SMCKO LdlrKO
ns
Lesion Area (μm2 X 105)
Adamts7SMCWT LdlrKO
Adamts7SMCKO LdlrKO
D
Adamts7ECWT LdlrKO
VS.
Adamts7ECKO LdlrKO
Adamts7 f/f LdlrKO
Adamts7 f/f LdlrKO Cdh5-CreERT2
7 Weeks Old Tamoxifen
8 Weeks Old Diet Initiation
16 Weeks of Western Diet
Harvest
E
Adamts7ECWT LdlrKO
Adamts7ECKO LdlrKO
ns
% Lesion
Adamts7ECWT LdlrKO
Adamts7ECKO LdlrKO
F
Adamts7ECWT LdlrKO
Adamts7ECKO LdlrKO
ns
Lesion Area (μm2 X 105)
Adamts7ECWT LdlrKO
Adamts7ECKO LdlrKO

Figure 2. SMC or EC knockout of *Adamts7* does not affect atherosclerosis. (A) Schematic outlining experimental design and mouse comparisons for SMC knockout of *Adamts7*. Created with BioRender.com (B) Representative ORO staining of en-face aortas and enumeration. n = 14, 12. (C) Representative images of hematoxylin and eosin (H&E) stained aortic root sections, quantification of plaque areas n = 5,7. Scale bar = 500um. (D) Schematic outlining experimental design and mouse comparisons for EC knockout of *Adamts7*. Created with BioRender.com (E) Representative ORO staining of en-face aortas and enumeration. n = 7. (F) Representative images of H&E stained aortic root sections, quantification of plaque areas n = 6,7. Scale bar = 500um. Statistics were analyzed using a 2-tailed Student's t-test.

FIGURE 3

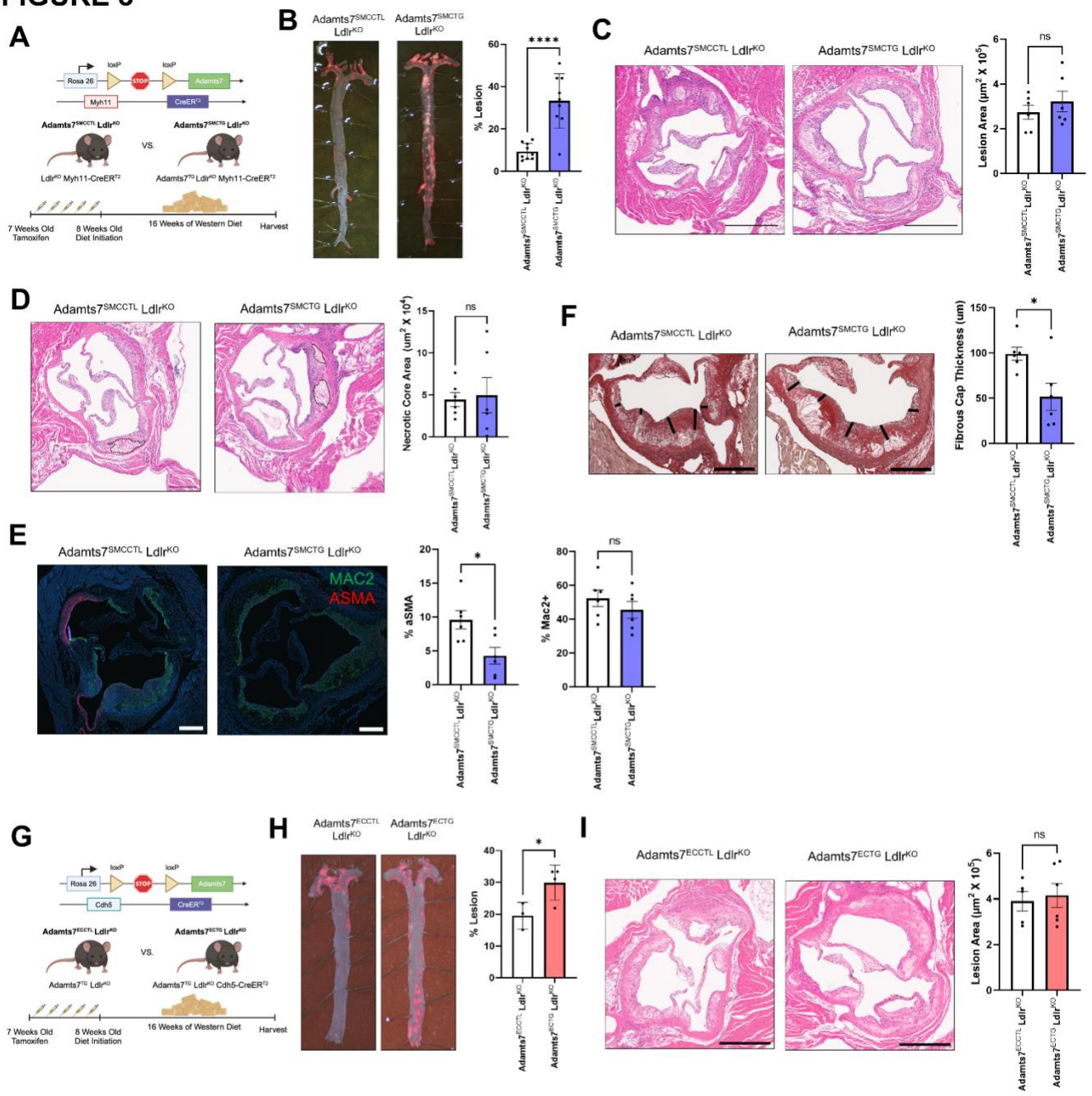
A
Rosa 26
loxP
STOP
loxP
Adamts7
Myh11
CreER^{T2}
Adamts7^{SMCCTL} Ldlr^{KO}
VS.
Adamts7^{SMCTG} Ldlr^{KO}
Ldlr^{KO} Myh11-CreER^{T2}
Adamts7^{TG} Ldlr^{KO} Myh11-CreER^{T2}
7 Weeks Old Tamoxifen
8 Weeks Old Diet Initiation
16 Weeks of Western Diet
Harvest
B
Adamts7^{SMCCTL} Ldlr^{KO}
Adamts7^{SMCTG} Ldlr^{KO}
% Lesion
****
C
Adamts7^{SMCCTL} Ldlr^{KO}
Adamts7^{SMCTG} Ldlr^{KO}
Lesion Area (μm^2 X 10^5)
ns
D
Adamts7^{SMCCTL} Ldlr^{KO}
Adamts7^{SMCTG} Ldlr^{KO}
Necrotic Core Area (um^2 X 10^4)
ns
F
Adamts7^{SMCCTL} Ldlr^{KO}
Adamts7^{SMCTG} Ldlr^{KO}
Fibrous Cap Thickness (um)
*
E
Adamts7^{SMCCTL} Ldlr^{KO}
Adamts7^{SMCTG} Ldlr^{KO}
MAC2
ASMA
% aSMA
*
% Mac2+
ns
G
Rosa 26
loxP
STOP
loxP
Adamts7
Cdh5
CreER^{T2}
Adamts7^{ECCTL} Ldlr^{KO}
VS.
Adamts7^{ECTG} Ldlr^{KO}
Adamts7^{TG} Ldlr^{KO}
Adamts7^{TG} Ldlr^{KO} Cdh5-CreER^{T2}
7 Weeks Old Tamoxifen
8 Weeks Old Diet Initiation
16 Weeks of Western Diet
Harvest
H
Adamts7^{ECCTL} Ldlr^{KO}
Adamts7^{ECTG} Ldlr^{KO}
% Lesion
*
I
Adamts7^{ECCTL} Ldlr^{KO}
Adamts7^{ECTG} Ldlr^{KO}
Lesion Area (μm^2 X 10^5)
ns

Figure 3. SMC and EC transgenic *Adamts7* increases aortic atherosclerosis. (A) Schematic outlining experimental design and the generation of the SMC Transgenic ADAMTS7 mouse. Created with BioRender.com (B) ORO staining of the en-face aorta and quantification of lesion area. n = 9. (C) Representative images of H&E stained aortic root sections, quantification of plaque areas n = 6. Scale bar = 500um. (D) Representative images of H&E stained aortic root sections with necrotic core outlined in dotted line n = 6 mice. Scale bar = 300um. (E) Representative images of aortic root sections stained against ASMA (Cy3 - red), MAC2 (AlexaFluor 488 - green), and cell nuclei (DAPI - blue) with their subsequent quantification relative to lesion area n = 6. Scale bar = 300um. (F) Representative picrosirius red staining of aortic root lesions with bars indicating fibrous cap thickness and quantification of fibrous cap thickness n = 6. Scale bar = 300um. (G) Schematic outlining experimental design and the generation of the EC Transgenic ADAMTS7 mouse. Created with BioRender.com (H) ORO staining of the en-face aorta and quantification of lesion area. n = 3,4. (I) Representative images of H&E stained aortic root sections, quantification of plaque areas n = 5,6. Scale bar = 500um. ****P<0.0001, ***P<0.001, ** P<0.01, *P<0.05. Statistics were analyzed using a 2-tailed Student's t-test.

FIGURE 4

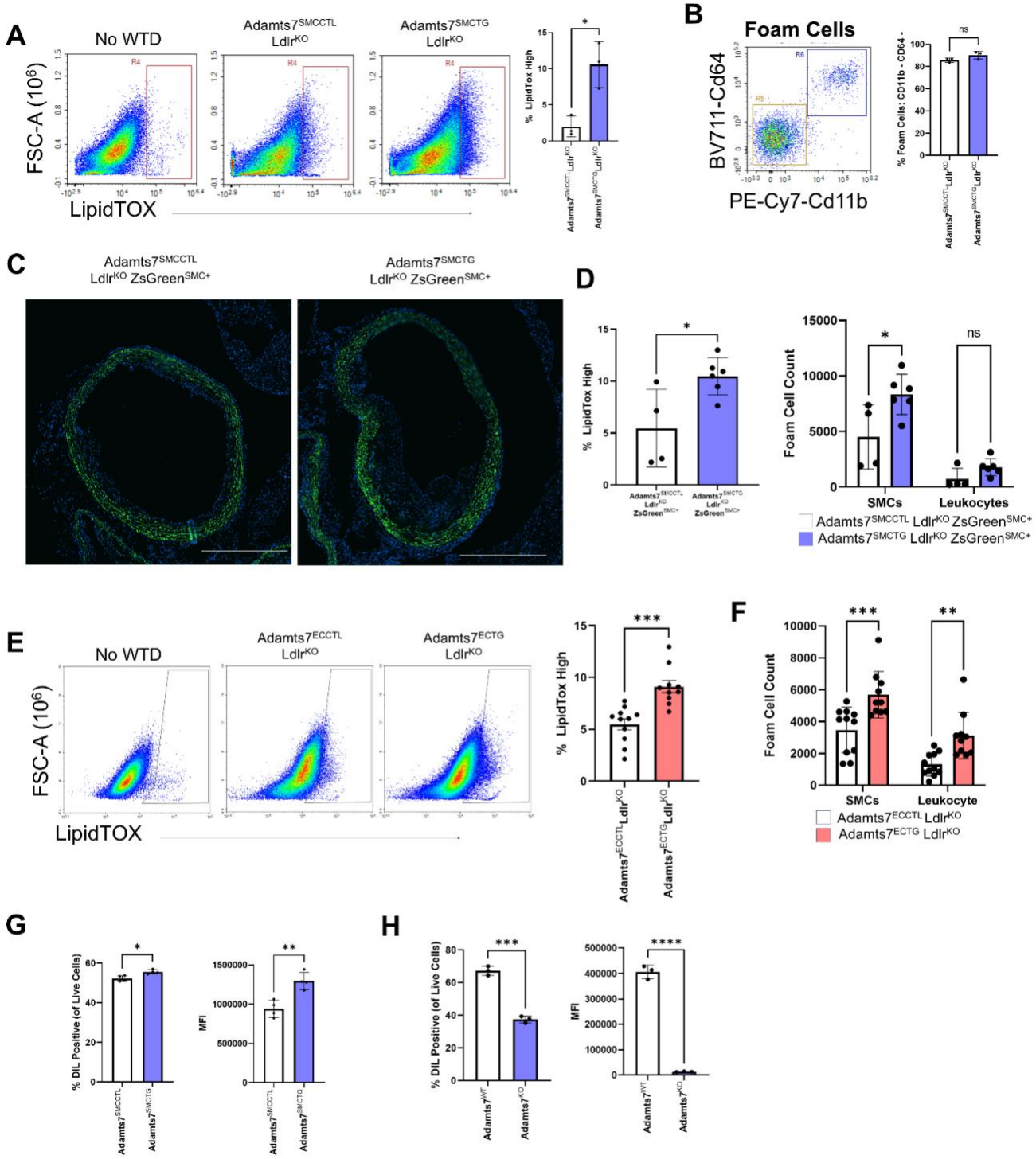
A
No WTD
Adamts7SMCCTL LdlrKO
Adamts7SMCTG LdlrKO
FSC-A (10^6)
LipidTOX
% LipidTox High
B
Foam Cells
BV711-Cd64
PE-Cy7-Cd11b
% Foam Cells: CD11b - CD64 -
ns
C
Adamts7SMCCTL LdlrKO ZsGreenSMC+
Adamts7SMCTG LdlrKO ZsGreenSMC+
D
% LipidTox High
Foam Cell Count
SMCs
Leukocytes
Adamts7SMCCTL LdlrKO ZsGreenSMC+
Adamts7SMCTG LdlrKO ZsGreenSMC+
E
No WTD
Adamts7ECCTL LdlrKO
Adamts7ECTG LdlrKO
FSC-A (10^6)
LipidTOX
% LipidTox High
F
Foam Cell Count
SMCs
Leukocyte
Adamts7ECCTL LdlrKO
Adamts7ECTG LdlrKO
G
% DIL Positive (of Live Cells)
MFI
H
% DIL Positive (of Live Cells)
MFI

Figure 4. ADAMTS7 promotes foam cell expansion. (A) Flow cytometry-based quantification of foam cells through LipidTOX staining of the aorta. A normolipidemic aorta was used to establish the LipidTOX high gate. n = 3 (B) Breakdown of foam cells stained positively for CD11B and CD64 n = 3. (C) Confirmation of efficient ZsGreen labeling of SMCs with nuclei counterstained with DAPI. Scale bar = 500um. (D) Foam cell analysis with the SMC lineage tracer ZsGreen and leukocyte marker CD45 after 12 weeks of WTD. Counts were normalized to 100,000 live cells. n = 4-6 mice. Statistics were analyzed by two-way ANOVA with Sidak's multiple comparison test. (E) Flow cytometry-based quantification of foam cells through LipidTOX staining of the aorta. A normolipidemic aorta was used to establish the LipidTOX high gate. n = 3-4. (F) Normalized foam cell counts out of 100,000 live cells after 16 weeks of WTD. Leukocytes were identified as CD45+. SMCs were identified as CD31- CD45- CD200+. n = 11-10 mice. Statistics were analyzed by two-way ANOVA with Sidak's multiple comparison test. (G) In vitro foam cell analysis with primary cells from transgenic mice treated with 10ug/mL Dil-oxLDL for 24 hours, n = 4. (H) In vitro foam cell analysis with explanted primary SMCs from whole body *Adamts7* knockout mice treated with 10ug/mL Dil-oxLDL for 24 hours, n = 3. ****P<0.0001, ***P<0.001, ** P<0.01, *P<0.05 Between sample comparisons were analyzed by a 2-tailed Student's t-test.

FIGURE 5

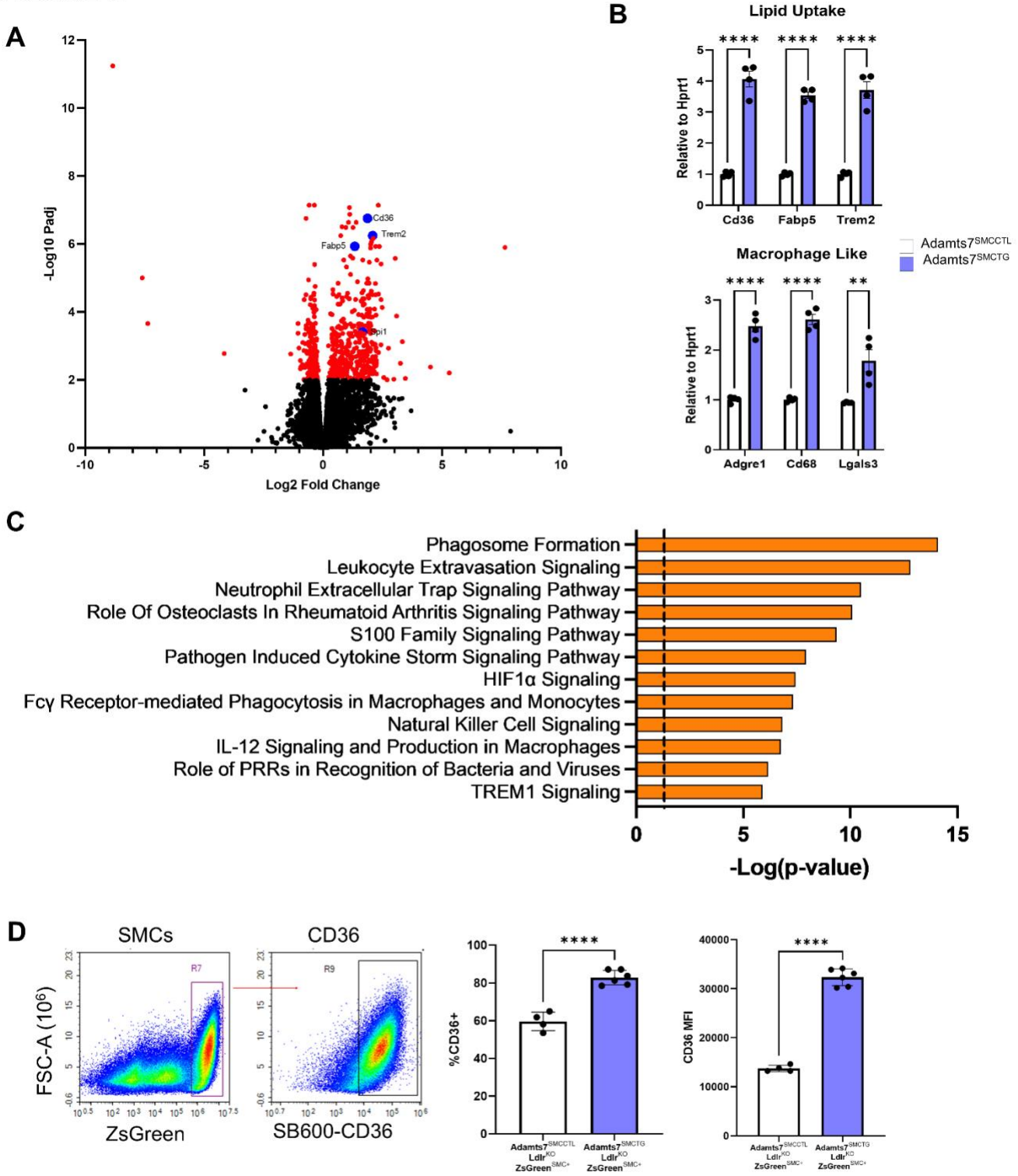
A
-Log10 Padj
Log2 Fold Change
Cd36
Trem2
Fabp5
Apoe
B
Lipid Uptake
Relative to Hprt1
Cd36
Fabp5
Trem2
Macrophage Like
Adgre1
Cd68
Lgals3
Adamts7SMCCTL
Adamts7SMCTG
C
Phagosome Formation
Leukocyte Extravasation Signaling
Neutrophil Extracellular Trap Signaling Pathway
Role Of Osteoclasts In Rheumatoid Arthritis Signaling Pathway
S100 Family Signaling Pathway
Pathogen Induced Cytokine Storm Signaling Pathway
HIF1α Signaling
Fcγ Receptor-mediated Phagocytosis in Macrophages and Monocytes
Natural Killer Cell Signaling
IL-12 Signaling and Production in Macrophages
Role of PRRs in Recognition of Bacteria and Viruses
TREM1 Signaling
-Log(p-value)
D
SMCs
CD36
FSC-A (10^6)
ZsGreen
SB600-CD36
%CD36+
CD36 MFI

Figure 5. Bulk RNAseq of *Adamts7*^{SMCTG} primary SMCs reveals an increase in lipid handling genes. (A) Volcano plot of the most upregulated and downregulated genes by *P* value adjusted for multiple comparisons. Passage two cells were used for RNAseq. (B) qRT-PCR confirmation of upregulated lipid uptake and macrophage-like genes n = 4. Normalization was performed relative to *Hprt1*. (C) Ingenuity Pathway Analysis of differentially expressed genes with Ingenuity Canonical Pathways highlighted. Shown pathways are predicted to be upregulated within *Adamts7*^{SMCTG} primary SMCs. (D) Confirmation of enhanced SMC CD36 in vivo. Flow cytometry analysis of lineage traced mice after 12 weeks of WTD feeding n = 4- 6 mice. ****P<0.0001, ** P<0.01 Statistics were analyzed using a 2-tailed Student's t-test.

FIGURE 6

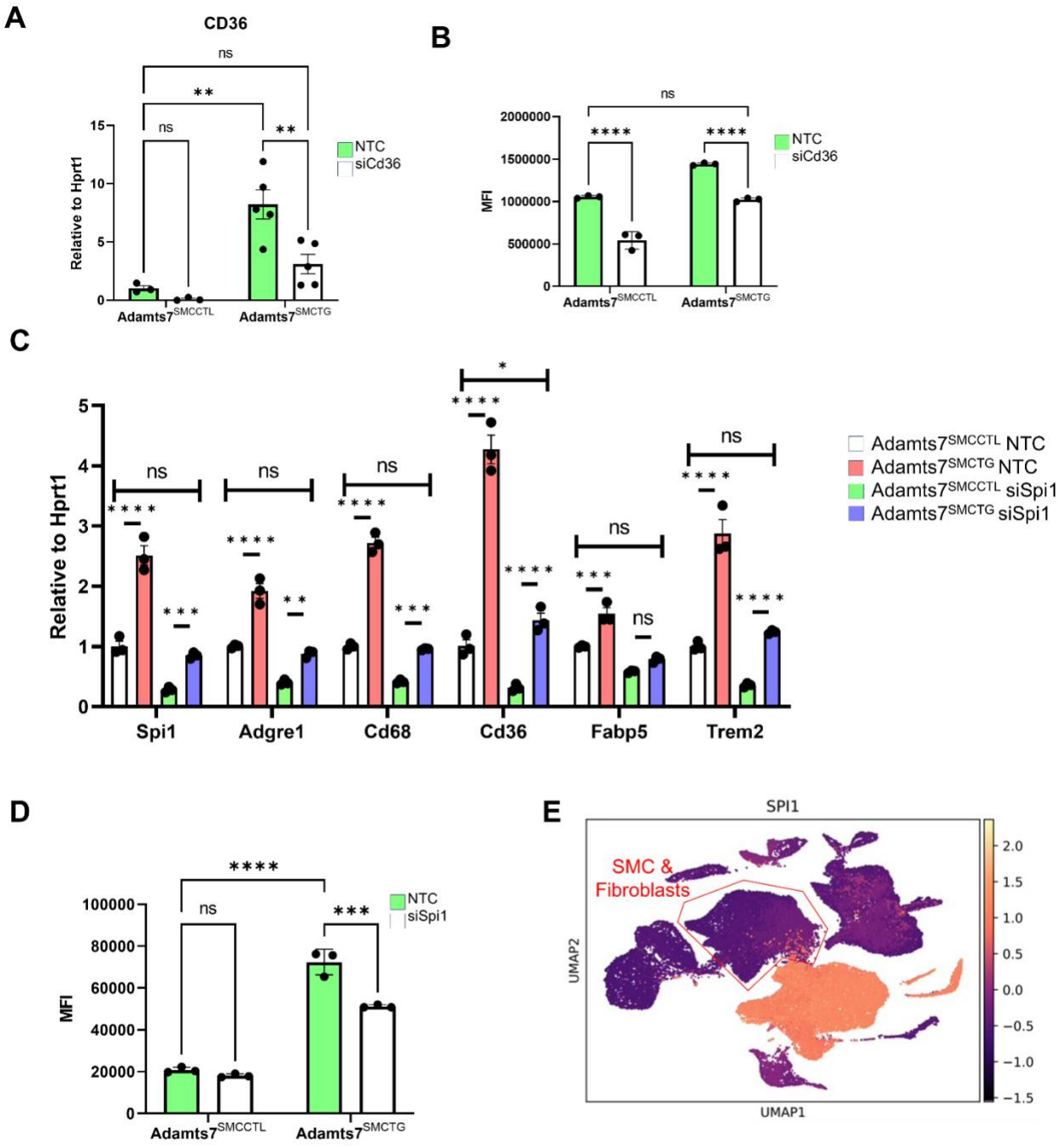
A
CD36
ns
**
ns
**
Relative to Hprt1
NTC
siCd36
Adamts7SMCCTL
Adamts7SMCTG
B
ns
****
****
MFI
NTC
siCd36
Adamts7SMCCTL
Adamts7SMCTG
C
Relative to Hprt1
Adamts7SMCCTL NTC
Adamts7SMCTG NTC
Adamts7SMCCTL siSpi1
Adamts7SMCTG siSpi1
Spi1
Adgre1
Cd68
Cd36
Fabp5
Trem2
D
MFI
NTC
siSpi1
Adamts7SMCCTL
Adamts7SMCTG
E
SPI1
SMC &
Fibroblasts
UMAP2
UMAP1

Figure 6. CD36 and PU.1 mediate ADAMTS7 conferred foam cell expansion. (A) Confirmation of knockdown of *Cd36* through siRNA. Primary SMCs were treated with 10nM of either an NTC or *Cd36* siRNA. Knockdown was assessed 48 hours after transfection n = 3-5 mice. (B) Flow analysis of oxLDL lipid uptake. 24 hours post siRNA transfection, cells were treated with 10ug/mL of Dil-oxLDL, and uptake was assessed 24 hours post oxLDL treatment n = 3. (C) Knockdown of *Spi1* in primary SMCs. Cells were treated with 10nM of siRNA, and 48 hours after transfection, cells were harvested for qRT-PCR. (D) Flow analysis of lipid uptake. 24 hours post *Spi1* siRNA transfection, cells were treated with 10ug/mL of Dil-oxLDL, and uptake was assessed 24 hours post oxLDL treatment. (E) Expression of *SPI1* in human carotid atherosclerosis. ****P<0.0001, ***P<0.001, ** P<0.01, *P<0.05 Statistics were analyzed by two-way ANOVA with Sidak's multiple comparison test.

Upstream Regulator	Expr Fold Change	Molecule Type	Activation z-score
lipopolysaccharide	-	chemical drug	5.491
TNF	-	cytokine	5.103
E. coli B4 lipopolysaccharide	-	chemical toxicant	4.872
tetradecanoylphorbol acetate	-	chemical drug	4.833
SPI1	**3.16**	**transcription regulator**	**4.682**
CSF2	-	cytokine	4.675
AGT	-	growth factor	4.593
OGA	-	enzyme	4.593
tretinoin	-	chemical drug	4.484
CNTF	-	cytokine	4.243
cardiotoxin	-	chemical - other	4.123
BHLHE40	**-**	**transcription regulator**	**4.022**
IL33	-	cytokine	3.943
SMARCA4	**-**	**transcription regulator**	**3.939**
CEBPA	**3.969**	**transcription regulator**	**3.913**
D-glucose	-	chemical - endogenous mammalian	3.907
USP22	-	peptidase	3.898
CD44	-	other	3.843
poly rI:rC-RNA	-	biologic drug	3.814
IFNG	-	cytokine	3.703
ITPR2	-	ion channel	3.592
TGM2	-	enzyme	3.568
bleomycin	-	biologic drug	3.567
KLF6	**-**	**transcription regulator**	**3.549**
dihydrotestosterone	-	chemical - endogenous mammalian	3.539

Table 1. IPA upstream regulator analysis to identify candidate transcription factors. Upstream regulator analysis of RNAseq reveals activated candidate molecules responsible for the gene expression changes. Five transcription factors are listed within the top 25 listed molecules.

SUPPLEMENTARY FIGURE 1

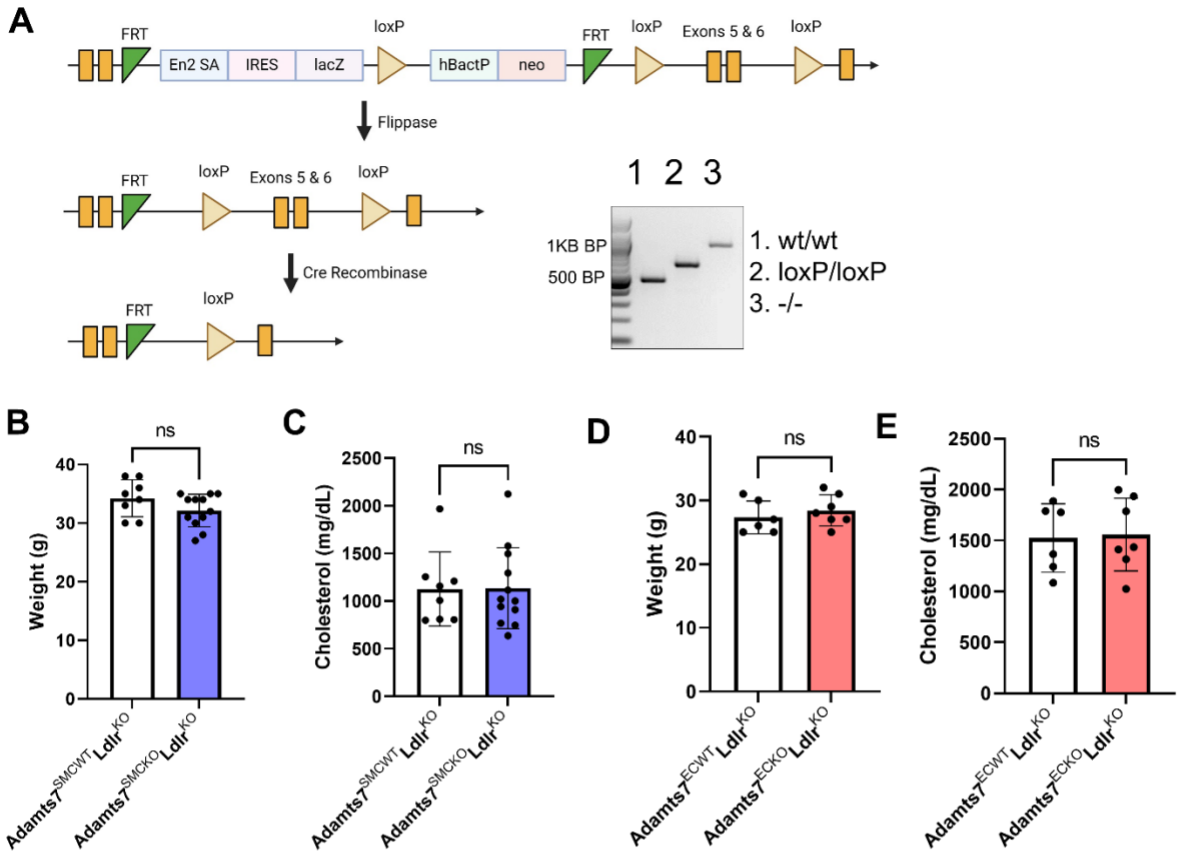

Figure S1. Design of conditional knockout mice and weights and cholesterol after WTD. (A) Schematic overview of the knockout-first allele. Knockout mice were crossed with the flp recombinase deleter mice, generating mice with floxed *Adamts7* exons 5 and 6. Subsequently, breeding the conditional knockout mice with a Cre recombinase produces tissue-specific *Adamts7* knockout. Genotyping of wild-type, conditional knockout, and whole-body knockout mice. (B) Mice's weight (grams) and (C) plasma total cholesterol (mg/dL) after 16 weeks of WTD feeding for *Adamts7*^{SMCWT} *Ldlr*^{KO} and *Adamts7*^{SMCKO} *Ldlr*^{KO} mice. n = 8-12 male mice. (D) Mice's weight (grams) and (E) plasma total cholesterol (mg/dL) after 16 weeks of WTD feeding for *Adamts7*^{ECWT} *Ldlr*^{KO} and *Adamts7*^{ECKO} *Ldlr*^{KO} mice. n = 6-7 female mice. Statistics were analyzed using a 2-tailed Student's t-test.

SUPPLEMENTARY FIGURE 2

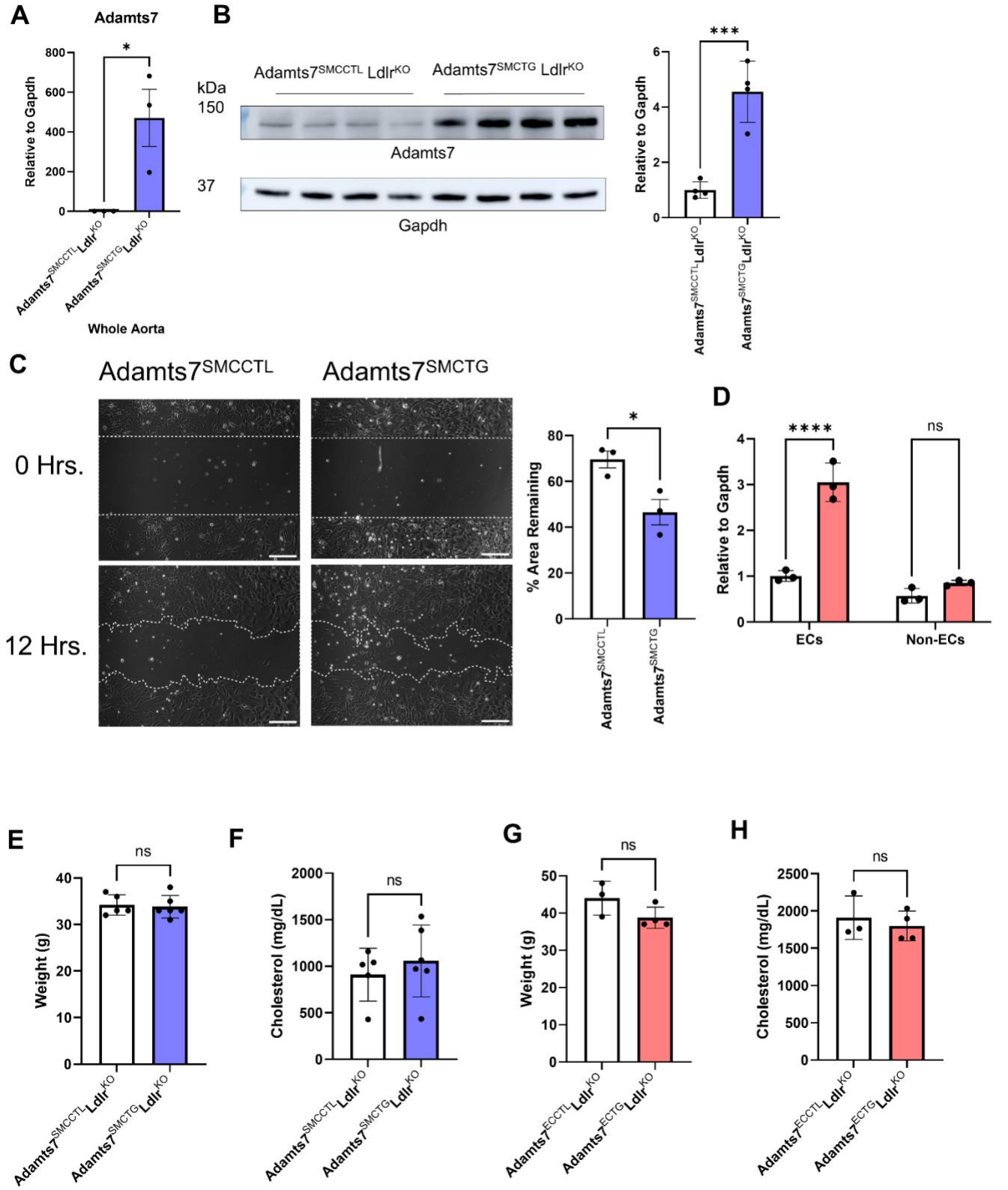

Figure S2. Verification and validation of transgenic mice. (A) Verification of *Adamts7* overexpression in Adamts7^{SMCTG} LdIr^{KO} mice by qPCR n = 3 male mice. (B) Validation of ADAMTS7 protein overexpression n = 4 male mice. (C) *Adamts7*^{SMCTG} mice have enhanced migration. n = 3 male mice. Scale bar = 200um (D) Verification of *Adamts7* transgenic expression in isolated mouse lung ECs (CD31+) and non-ECs (CD31-) n = 3. (E) Mice's weight (grams) and (F) plasma total cholesterol (mg/dL) after 16 weeks of WTD feeding for *Adamts7*^{SMCCTL} *Ldlr*^{KO} and *Adamts7*^{SMCTG} *Ldlr*^{KO} mice. n = 5-7 male mice. (G) Mice's weight (grams) and (H) plasma total cholesterol (mg/dL) after 16 weeks of WTD feeding for *Adamts7*^{ECCTL} *Ldlr*^{KO} and *Adamts7*^{ECTG} *Ldlr*^{KO} mice. n = 3-4 female mice. Statistics were analyzed using a 2-tailed Student's t-test.

SUPPLEMENTARY FIGURE 3

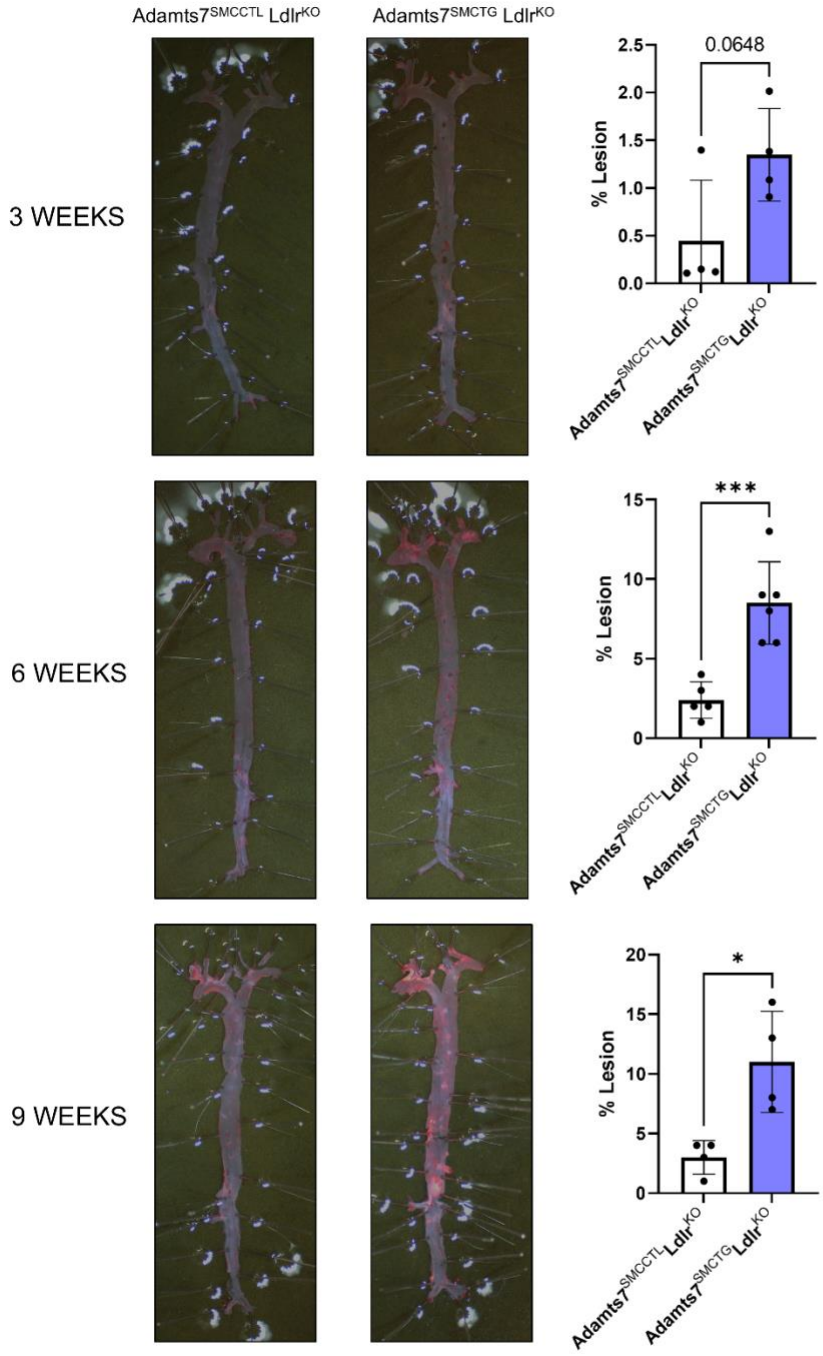

Figure S3. Increased atherosclerosis with short durations of WTD feeding in *Adamts7*^{SMCTG} mice. Representative images of ORO stained en-face aortas after three, six, and nine weeks of WTD feeding. *P < 0.05; ***P < 0.001 Statistics were analyzed using a 2-tailed Student's t-test.

SUPPLEMENTARY FIGURE 4

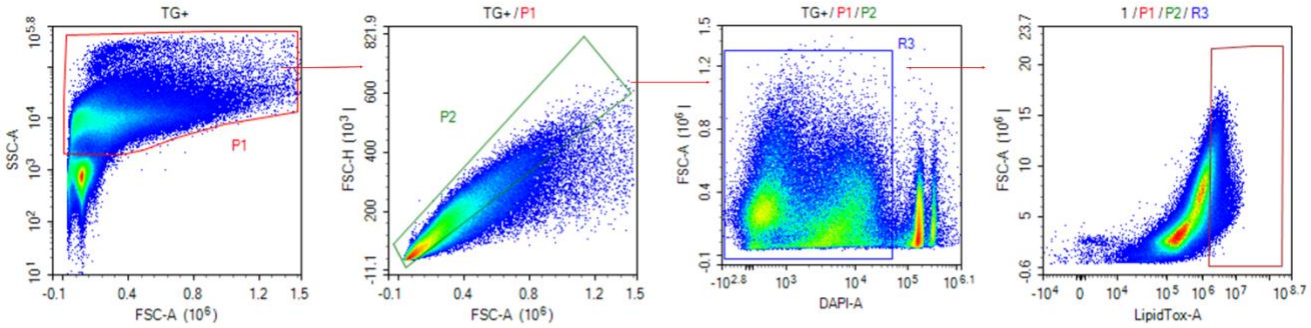

Figure S4. Representative gating strategy for foam cells.

Representative flow cytometry gating strategy. Cells were isolated from debris. Singlets and live cells (DAPI negative) were subsequently analyzed. LipidTOX high gate was established using a normal lipidemic C57BL6J aorta.

SUPPLEMENTARY FIGURE 5

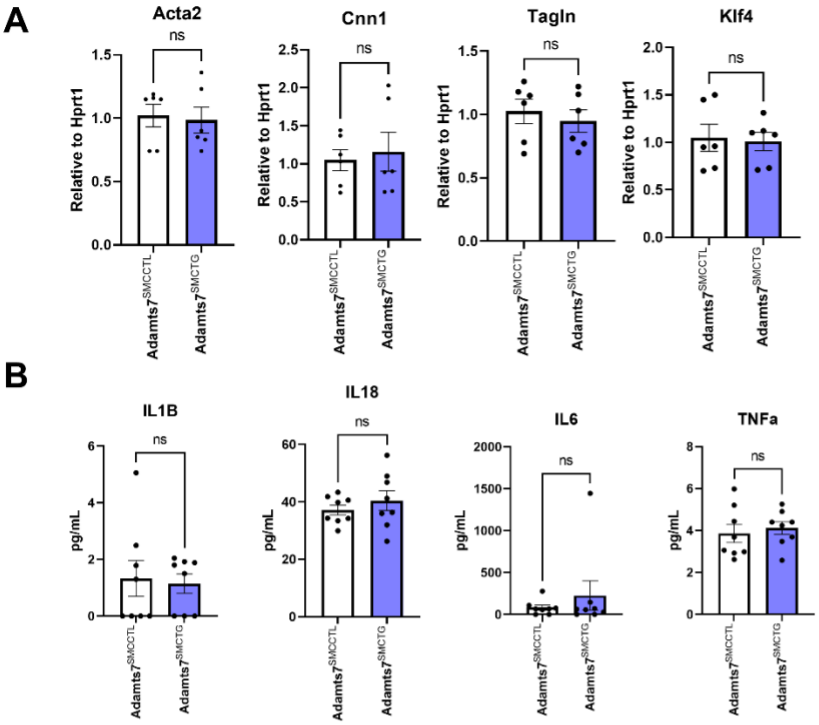

Figure S5. Characterization of explanted primary SMCs

(A) qPCR characterization of contractile and modulated genes. n = 6. (B) LEGENDplex-based ELISA is used to detect inflammatory cytokines in cell culture-conditioned media. Cells were from n = 8 mice. Statistics were analyzed using a 2-tailed Student's t-test.

SUPPLEMENTARY FIGURE 6

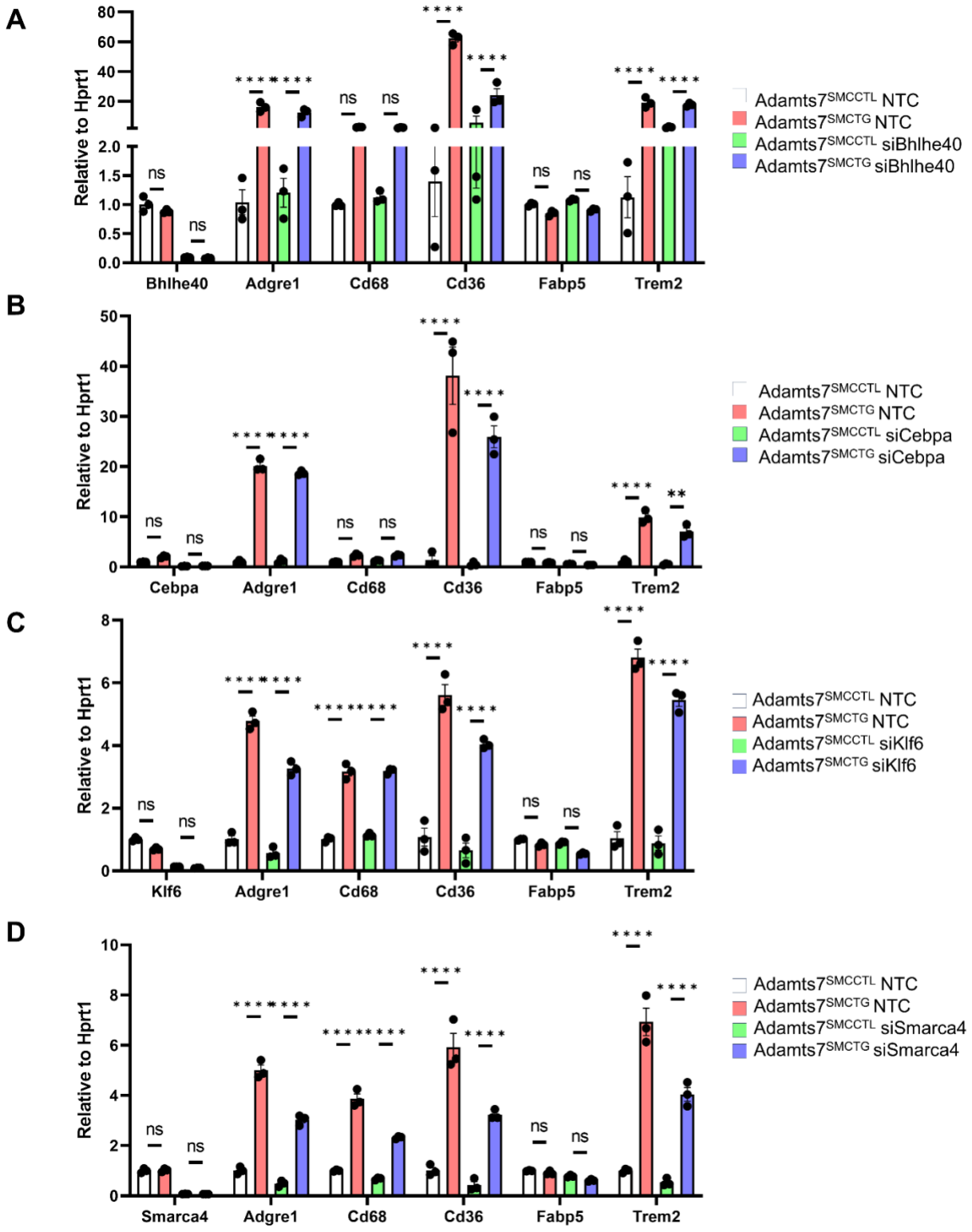

Figure S6. Knockdown of candidate transcription factors does not alter *Adamts7* conferred macrophage-like and lipid-handling genes.

Indicated siRNAs (10nM) were used to knock down candidate transcription factors in primary SMCs from *Adamts7*^{SMCCTL} and *Adamts7*^{SMCTG} mice. 48 hours after transfection, cells were harvested for qRT-PCR analysis. ****P<0.0001, ***P<0.001, ** P<0.01, *P<0.05 by two-way ANOVA with Sidak's multiple comparison test.